Photosynthesis-assisted remodeling of three-dimensional printed structures

Kunhao Yu[a,1], Zhangzhengrong Feng[a,1], Haixu Du[a], An Xin[a], Kyung Hoon Lee[a], Ketian Li[a], Yipin Su[a], Qiming Wang[a,2], Nicholas X. Fang[b,2], and Chiara Daraio[c,2]

[a]Sonny Astani Department of Civil and Environmental Engineering, University of Southern California, Los Angeles, CA 90089; [b]Department of Mechanical Engineering, Massachusetts Institute of Technology, Cambridge, MA 02139; and [c]Division of Engineering and Applied Science, California Institute of Technology, Pasadena, CA 91125

Edited by Zhigang Suo, Harvard University, Cambridge, MA, and approved December 10, 2020 (received for review August 4, 2020)

The mechanical properties of engineering structures continuously weaken during service life because of material fatigue or degradation. By contrast, living organisms are able to strengthen their mechanical properties by regenerating parts of their structures. For example, plants strengthen their cell structures by transforming photosynthesis-produced glucose into stiff polysaccharides. In this work, we realize hybrid materials that use photosynthesis of embedded chloroplasts to remodel their microstructures. These materials can be used to three-dimensionally (3D)-print functional structures, which are endowed with matrix-strengthening and crack healing when exposed to white light. The mechanism relies on a 3D-printable polymer that allows for an additional cross-linking reaction with photosynthesis-produced glucose in the material bulk or on the interface. The remodeling behavior can be suspended by freezing chloroplasts, regulated by mechanical preloads, and reversed by environmental cues. This work opens the door for the design of hybrid synthetic-living materials, for applications such as smart composites, lightweight structures, and soft robotics.

3D printing | self-remodeling | self-strengthening | self-healing | photosynthesis

Plants can grow and form complex, hierarchical structures that are challenging to reproduce with traditional engineering practices (1). Plant cells use photosynthesis to produce glucose, which is delivered to selected locations, such as trunks and crotches. Glucose, in turn, is used to form stiff polysaccharides (e.g., cellulose, chitosan, and chitin), which remodel and strengthen the plant structures locally (Fig. 1*A*) (2, 3). For example, the stiffness of a young stem is typically on the order of kilopascal, while the stiffness of a mature trunk can reach as high as several gigapascals (4). Mechanical loads are found to augment the strengthening of the plant structure through mechanotransduction pathways (5). In recent years, the availability of three-dimensional (3D)-printing technologies has driven the fabrication of engineering structures that attempt to mimic the complexity of the plants' architectures (6–10). However, how to mimic the plants' ability to remodel their components and strengthen mechanical properties remains elusive. Synthetic structures, on the contrary, typically weaken during service life because of materials fatigue or degradation. Developing hybrid, 3D-printable materials that exploit living photosynthesis processes to remodel their structures would be a major leap forward in engineering materials that mimic natural systems. However, establishing a communication channel between the synthetic 3D-printable materials and the natural photosynthesis process is challenging.

Here, we present a class of 3D-printable polymers that can be remodeled by the photosynthesis of embedded chloroplasts to enable matrix strengthening and crack healing. With local light exposure, the polymers harness photosynthesis-produced glucose to facilitate an additional cross-linking reaction, forming a stiff region with "artificial polysaccharides" (Fig. 1*B*). The region with additional cross-links features enhanced Young's modulus, tensile strength, and fracture toughness by factors of 300–620%, compared to the region without the additional cross-links. Such photosynthesis-assisted strengthening can be suspended by freezing living chloroplasts, regulated by external mechanical preloads, and reversed by cleaving glucose cross-linkers with environmental cues. We also show that the photosynthesis-assisted strengthening can be applied to 3D-printed structures through patterned light and patterned loads. In addition, the photosynthesis can equip the 3D-printed structures with a healing capability via glucose-enabled interfacial cross-linking. The paradigm in this work provides a unique platform for remodeling engineering materials via the communication between synthetic polymers and natural photosynthesis processes.

Mechanism of Photosynthesis-Assisted Strengthening

To design a polymer network that allows for an additional cross-linking reaction with the photosynthesis-produced glucose, we design a polymer resin that features both acrylate and isocyanate distal groups (NCO) and then blend the resin with chloroplasts extracted from spinach leaves (*SI Appendix*, Figs. S1 and S2) (11). The acrylate groups can be utilized for the photopolymerization-based 3D printing (such as stereolithography), because the acrylate groups allow for a photoinitiated addition reaction to polymerize the resin (*SI Appendix*, Fig. S3) (12, 13). The printing is rapid with a speed of 75–400 μm/s, and the resolution can reach as

Significance

Living creatures are continuous sources of inspiration for designing engineering materials and structures. However, synthetic engineering materials are typically different from living creatures, because the latter consist of living cells to support their metabolisms, such as remodeling, growth, and reproduction. How to harness living cells to metabolize synthetic engineering materials remains largely elusive. Here, we report an attempt to exploit living chloroplasts to metabolize three-dimensional-printed polymers. With living chloroplasts and synthetic polymers, the system leads to a class of hybrid synthetic-living materials whose microstructures and properties can be remodeled on-demand by the photosynthesis of chloroplasts.

Author contributions: K.Y., Z.F., Q.W., N.X.F., and C.D. designed research; K.Y., Z.F., H.D., A.X., K.H.L., K.L., Y.S., and Q.W. performed research; K.Y., Z.F., H.D., A.X., K.H.L., K.L., Y.S., and Q.W. contributed new reagents/analytic tools; K.Y., Z.F., Q.W., N.X.F., and C.D. analyzed data; K.Y., Z.F., H.D., A.X., K.H.L., K.L., Y.S., Q.W., N.X.F., and C.D. wrote the paper; and Q.W. conceived the idea and supervised the team.

Competing interest statement: The University of Southern California has filed a patent application related to the work described here.

This article is a PNAS Direct Submission.

[1]K.Y. and Z.F. contributed equally to this work.

[2]To whom correspondence may be addressed. Email: qimingw@usc.edu, nicfang@mit.edu, or daraio@caltech.edu.

This article contains supporting information online at https://www.pnas.org/lookup/suppl/doi:10.1073/pnas.2016524118/-/DCSupplemental.

Published January 11, 2021.

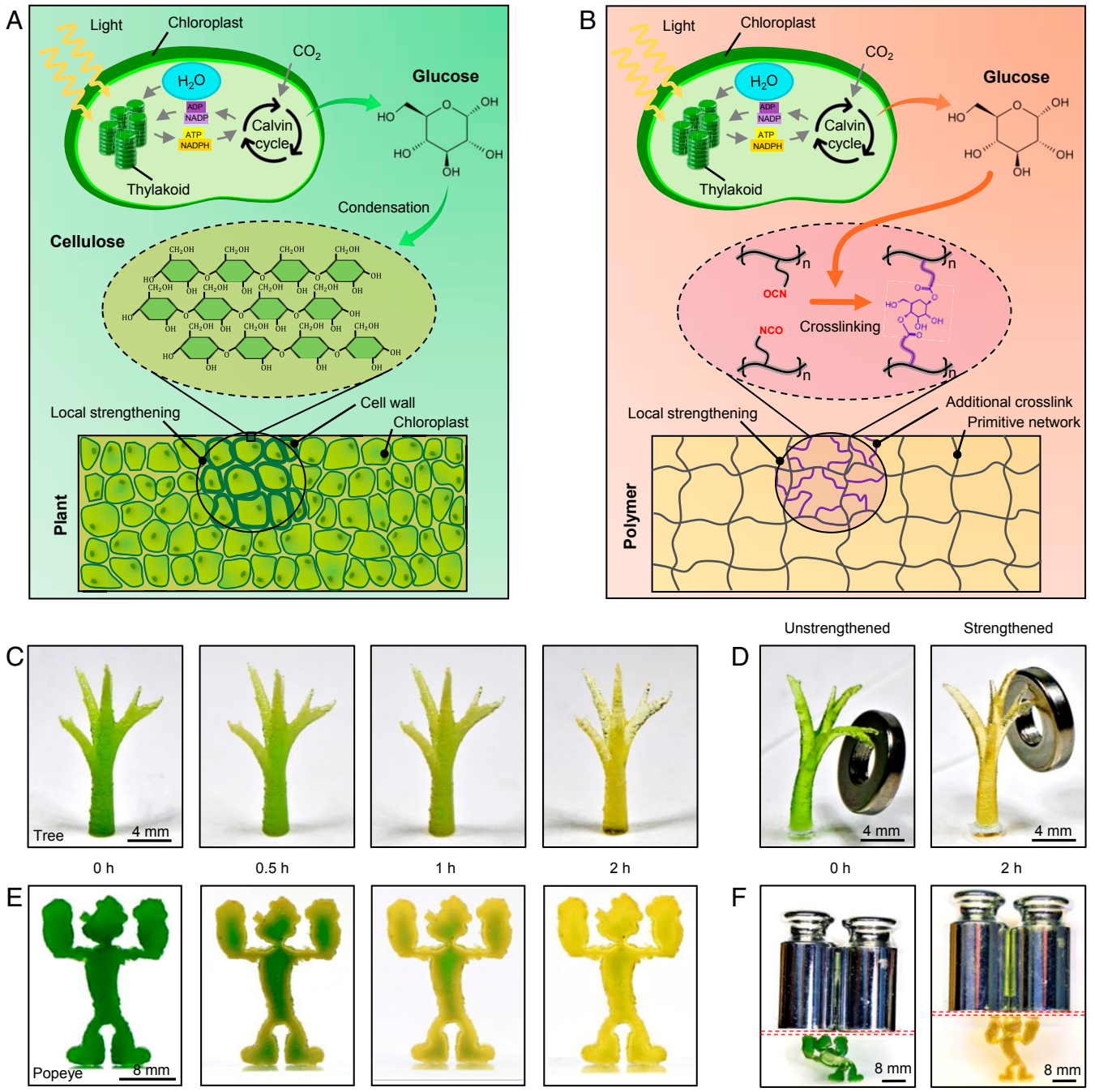

Fig. 1. Concept of the photosynthesis-assisted remodeling of 3D-printed structures. (*A*) Schematics to illustrate photosynthesis-assisted remodeling of plants. The photosynthesis-produced glucose undergoes a condensation reaction to form stiff polysaccharide (e.g., cellulose). (*B*) Schematics to illustrate photosynthesis-assisted remodeling of a synthetic polymer. The photosynthesis-produced glucose undergoes a reaction with isocyanate (NCO) side groups to form additional cross-links. (*C*) Image sequence of a 3D-printed treelike structure with various light illumination periods (white light intensity 69.3 W/m^2) of the photosynthesis process. (*D*) Unstrengthened and strengthened 3D-printed treelike structures loaded by the same weight (1 g). (*E*) Image sequence of a 3D-printed Popeye-like structure with various light illumination periods of the photosynthesis process. (*F*) Unstrengthened and strengthened 3D-printed Popeye-like structures loaded by the same weight (200 g). The red dashed boxes denote glass slides. The unstrengthened Popeye's height reduces by 34.7%, but the strengthened Popeye only by 7% (*SI Appendix*, Fig. S7).

low as ~25 μm. After the 3D-printing process, the NCO groups become free side groups within the polymer matrix (*SI Appendix*, Fig. S4). The NCO groups can enable a relatively strong reaction with hydroxyl groups (OH) on a glucose molecule to form urethane linkages (-NH-CO-O-) (Fig. 1*B* and *SI Appendix*, Fig. S4) (14). Since a glucose molecule has multiple OH groups, it is hypothesized that the OH groups on the chloroplast-produced glucose can bridge multiple NCO groups to create new cross-links additional to the acrylate-enabled cross-links within the polymer matrix (Fig. 1*B* and *SI Appendix*, Fig. S4). Such additional cross-links are expected to significantly enhance the modulus and strength of the polymer (15, 16).

To demonstrate the strengthening concept, we 3D-print a treelike structure whose Young's modulus and tensile strength

gradually increase as the photosynthesis illumination period increases (white light intensity 69.3 W/m^2, Fig. 1*C* and *SI Appendix*, Fig. S5). The strengthened structure with 2-h illumination shows a better weight-sustaining capability than the unstrengthened structure (Fig. 1*D* and *SI Appendix*, Fig. S6). Note that the photosynthesis process includes 2-h illumination of white light for glucose generation plus 2-h darkness for glucose exportation from the chloroplast (11, 17, 18). As an educational example, we 3D-print Popeye the Sailor, an American cartoon character who can strengthen his muscles by eating spinach (Fig. 1*E*). We show that the 3D-printed Popeye-like structure strengthens upon light exposure, by leveraging the photosynthesis process of the embedded spinach chloroplasts (2-h illumination and 2-h darkness). We demonstrate the strengthening effect by showing a reduced deformation upon loading (Fig. 1*F* and *SI Appendix*, Fig. S7).

We follow three steps to verify the hypothesized mechanism of photosynthesis-assisted strengthening (Fig. 2). In step 1, we verify that both light and chloroplasts are required to strengthen the designed polymer. We study three sample groups for comparison: The experimental group includes polymer samples with free NCO groups and embedded chloroplasts, going through 4-h illumination and 4-h darkness (Fig. 2*A*). To verify the effect of light, we employ control 1 group that includes polymer samples with free NCO groups and embedded chloroplasts, going through 8-h darkness (Fig. 2*B*). To verify the effect of chloroplasts, we employ control 2 group that includes polymer samples with free NCO groups but without chloroplasts, going through 4-h light illumination and 4-h darkness (Fig. 2*C*). We present the differences among these groups in three aspects. First, from the sample color, the initially green experimental samples turn to pale yellow, because light illumination can transform green chlorophyll to yellow lutein (Fig. 2*D*) (19). In contrast, control 1 and 2 samples remain green and semitransparent, respectively (Fig. 2 *E* and *F*). Second, since the photosynthesis-produced glucose is expected to consume free NCO groups to form additional cross-links, the concentration reduction of free NCO groups can reveal the occurrence of the cross-linking reaction. To indicate the concentration of free NCO groups within the polymer matrix, we employ a Fourier transform infrared (FTIR) spectrometer to measure the transmittance of the sample around 2,260 cm^{-1} that is corresponding to the NCO bond-stretching vibration (13). We find an evident peak at 2,260 cm^{-1} in the initial state of all three sample groups (Fig. 2 *D*–*F*). After the respective processes, the peak of the experimental group drastically drops, indicating the decreasing of the NCO concentration (Fig. 2*D* and *SI Appendix*, Fig. S8*A*); however, the peaks of controls 1 and 2 remain almost the same (Fig. 2 *E* and *F* and *SI Appendix*, Fig. S8 *B* and *C*). Third, we compare the mechanical properties of three sample groups via uniaxial tensile tests (Fig. 2*G*). Compared to controls 1 and 2, the experimental group exhibits higher Young's modulus and tensile strength by factors of 620 and 350%, respectively (Fig. 2*H* and *SI Appendix*, Fig. S9*A*). Since the strengthening is due to the formation of additional permanent covalent cross-links, the strengthened Young's modulus and tensile strength do not degrade within at least 6 mo (*SI Appendix*, Fig. S10). We further find that the fracture energy of the experimental sample is almost three times those of controls 1 and 2 (Fig. 2*H* and *SI Appendix*, Figs. S9*B* and S11) (20, 21). The toughening mechanism is similar to that in particle-reinforce composites, because the regions around chloroplast fillers are strengthened by forming new cross-links.

Note that the required water for the photosynthesis process is supplied by the water storage within the chloroplasts (17, 18), and the required carbon dioxide is supplied by the existing carbon dioxide within the matrix and diffusion from the atmosphere (22). A rough estimation shows these supplies of water and carbon dioxide are sufficient for the experiments (*SI Appendix*, Table S1).

In step 2, we verify that chloroplasts can generate and export glucose to the polymer matrix. To detect the exported glucose within the polymer matrix, we employ a polymer sample with embedded chloroplasts but without free NCO groups (*SI Appendix*, Fig. S12). FTIR spectra show that the concentration of the OH group (3,300–3,500 cm^{-1}) (23) increases in the matrix after the photosynthesis process, implying the existence of free glucose that is not consumed by NCO groups (*SI Appendix*, Fig. S13).

In step 3, we verify that glucose can directly strengthen the designed polymer with free NCO groups but without chloroplasts. FTIR spectra show that the peak for the NCO groups disappears when glucose concentration is sufficiently high (e.g., 0.398 M), indicating that the glucose completely consumes the free NCO groups (*SI Appendix*, Fig. S14). Tensile tests show that both Young's moduli and tensile strengths increase as the glucose concentration increases (*SI Appendix*, Fig. S15).

Next, we study the effects of two vital factors on the strengthening performance: concentration of embedded chloroplasts and light illumination period (Fig. 2 *I* and *J*). First, we investigate polymer samples with chloroplasts of various weight concentrations (0–7 wt %) and free NCO groups (processed with 4-h illumination and 4-h darkness). Tensile stress–strain curves show that both Young's moduli and tensile strengths first increase with increasing chloroplast concentrations over 0–5 w t%, and then decrease afterward (5–7 wt %) (Fig. 2*I* and *SI Appendix*, Fig. S16*A*). The decrease after 5 wt % is probably because the chloroplasts serve as soft fillers within the polymer matrix, and a high concentration of soft fillers compromises the mechanical properties of the chloroplast-embedded polymer. Second, we employ various light illumination periods (white-light intensity 69.3 W/m^2) to process the polymer samples with 5 wt % chloroplasts and free NCO groups. Tensile stress–strain curves show that both Young's moduli and tensile strengths first increase (or reach a plateau) with increasing illumination time within 0–4 h, and then decrease afterward (4–6 h) (Fig. 2*J* and *SI Appendix*, Fig. S16*B*). The decrease after 4 h is probably because extralong illumination time may degrade the chloroplasts, associated with a reduction of the exported glucose concentration within the polymer matrix (similar behaviors for both 5 wt % (Fig. 2*J*) and 7 wt % of chloroplasts (*SI Appendix*, Fig. S16*C*)) (17, 18). Note that the effects of the chloroplast concentration and illumination period can be quantitatively explained by a theory that models the free energy of polymer networks with additional cross-links (*SI Appendix*, Figs. S17–S22 and Table S2).

A key difference between the presented hybrid synthetic-living material and the existing synthetic material is that the material property can be modulated by tuning the living activity of the involved biological element (i.e., chloroplast). Here, we employ a chilling temperature (0–4 °C) to temporarily freeze the activity of the embedded chloroplasts (24), and thus the material remains at the soft state after 2-h illumination and 2-h darkness (Fig. 2*K* and *SI Appendix*, Fig. S23 *A*–*C*). Once the temperature returns to 25 °C, the material can be strengthened to the stiff state via the photosynthesis process. This temporary freezing behavior cannot be achieved using traditional photoresins without living elements (*SI Appendix*, Fig. S23 *D*–*F*).

Another interesting feature of the presented material is that the photosynthesis-assisted strengthening can be reversed by cleaving the glucose cross-linkers with periodic acids (Fig. 2*L* and *SI Appendix*, Fig. S24) (25). With 2 M periodic acid, the Young's modulus and tensile strength of the initially strengthened polymer (with 4-h illumination and 4-h darkness) are reduced by 61 and 51%, respectively.

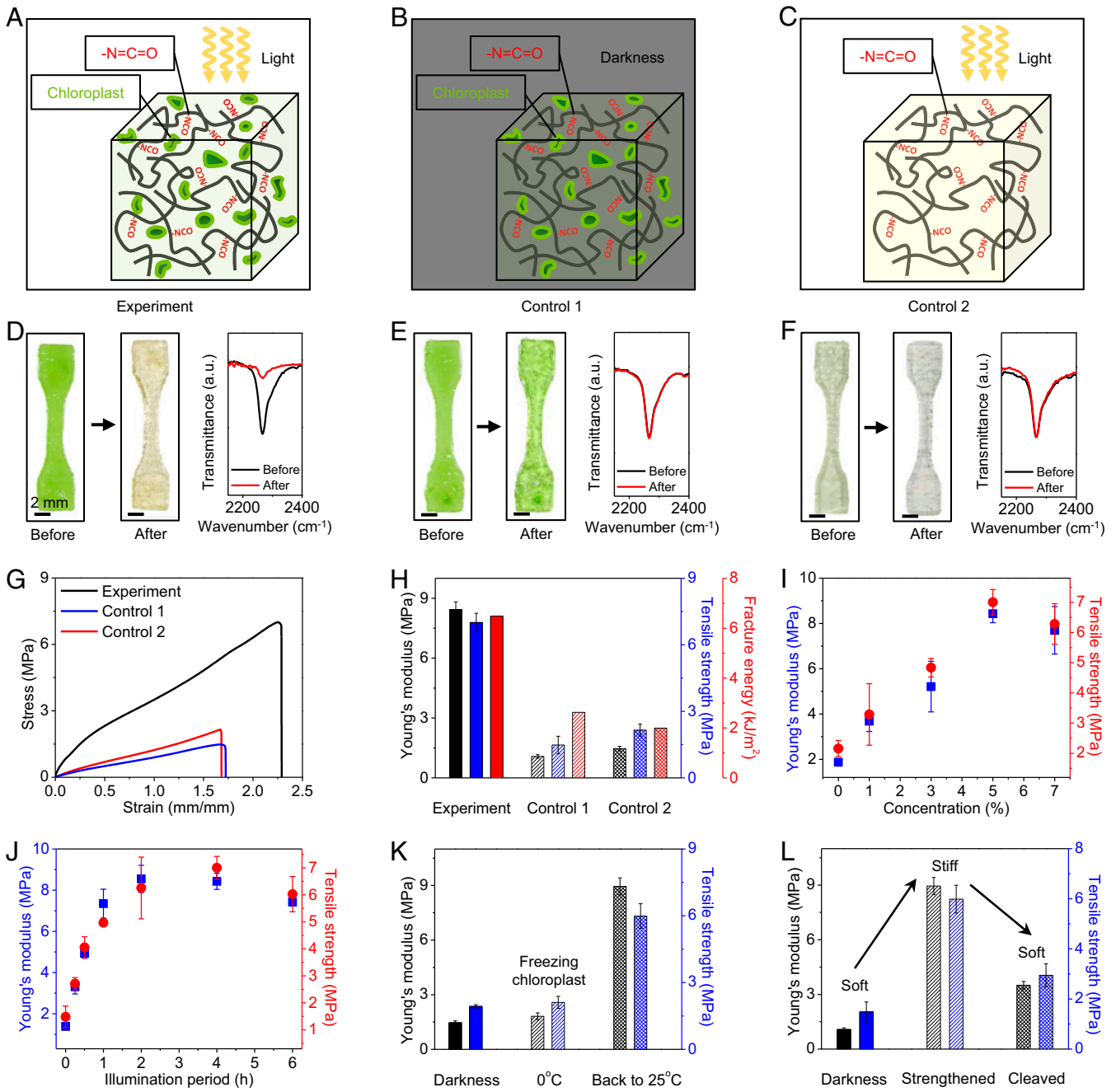

Fig. 2. Mechanism of photosynthesis-assisted strengthening. (*A*) Schematic of an experimental sample with free NCO groups and embedded chloroplasts undergoing 4-h light illumination and 4-h darkness. (*B*) Schematic of a control 1 sample with free NCO groups and embedded chloroplasts undergoing 8-h darkness. (*C*) Schematic of a control 2 sample with free NCO groups but without chloroplasts undergoing 4-h light illumination and 4-h darkness. (*D–F*) Samples and FTIR spectra before and after respective processes for (*D*) experiment, (*E*) control 1, and (*F*) control 2 cases, respectively. (*G*) Uniaxial tensile stress–strain curves of three groups of samples. (*H*) Young's moduli, tensile strengths, and fracture toughnesses of three groups of samples. (*I*) Young's moduli and tensile strengths of experimental samples with embedded chloroplasts of various weight concentrations (processed with 4-h illumination and 4-h darkness). (*J*) Young's moduli and tensile strengths of experimental samples with 5 wt % chloroplasts after the photosynthesis processes with various light illumination periods. (*K*) Young's moduli and tensile strengths of the processed experimental samples at three states: after 4-h darkness, after 2-h light and 2-h darkness at 0 °C, and after 2-h light and 2-h darkness at 0 °C followed by 2-h light and 2-h darkness at 25 °C. (*L*) Young's moduli and tensile strengths of processed experimental samples at three states: after 8-h darkness, strengthened with 4-h light illumination and 4-h darkness, and strengthened and treated with 2 M HIO_4 solution to cleave the glucose cross-linkers. Error bars in *H–L* represent SDs of 3–5 samples.

Photosynthesis-Assisted Strengthening with Patterned Light

Next, we show that the photosynthesis-assisted strengthening can be tuned by patterned light (Fig. 3). We demonstrate localized strengthening by exposing a plate sample to a patterned light with an "S" shape (Fig. 3*A*). After the photosynthesis with 4-h illumination and 4-h darkness, the illuminated S-shaped region turns from green to pale yellow (Fig. 3*B* and *SI Appendix*, Fig. S25). Indentation tests show that the average stiffness of the strengthened region is around 4.3 times that of the unstrengthened region (Fig. 3*C* and *D* and *SI Appendix*, Fig. S26). This local strengthening capability can be

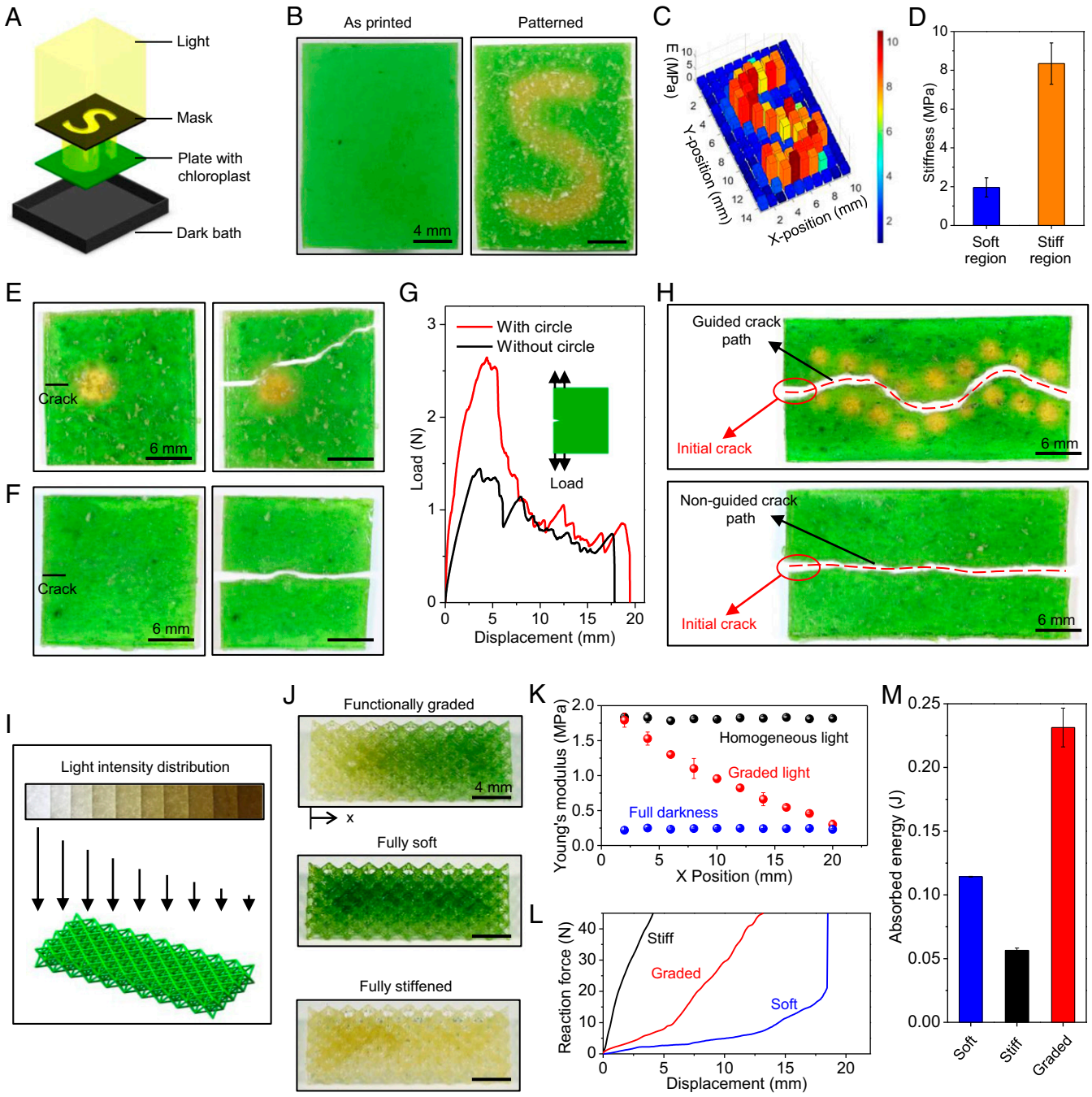

Fig. 3. Photosynthesis-assisted strengthening with patterned light. (*A*) Schematic of an experimental setup for the localized strengthening through a patterned light with an S shape. (*B*) Samples at the as-printed state and after 4-h illumination with an S-shaped light and 4-h darkness. (*C*) Young's modulus distribution of the patterned sample measured with indentation tests. (*D*) Average stiffness of the unstrengthened and strengthened regions. (*E*) Crack detouring in a plate sample with a strengthened circle. (*F*) Straight crack in a plate sample without a strengthened circle. (*G*) Load-displacement curves of samples with and without the strengthened circle. (*Inset*) The loading setup. (*H*) Crack paths of samples with and without wavy strengthened regions. (*I*) Schematic to illustrate a 3D-printed lattice structure processed by a graded light (*Left* to *Right*: 69.3–0 W/m^2). (*J*) Samples of functionally graded, fully soft, and fully stiffened lattices. (*K*) Effective Young's modulus distribution of three samples measured with indentation tests. (*L*) Compressive force-displacement curves of three samples with a loading rate of 10 mm/s. The loading is along the longitudinal gradient direction (x direction). (*M*) The absorbed energy of the three samples. The error bars in *D* and *M* represent SDs of 3–5 samples. Note that the inhomogeneous green color in *E*, *F*, and *H* is possibly due to some clusters of broken chloroplasts produced during the extraction experiments, which do not influence the result quality.

harnessed to detour crack paths within the material (Fig. 3 *E*–*H*). Due to the higher fracture toughness in the strengthened region, an initially straight crack detours a strengthened circle. The load-displacement curve shows that the toughness of the material is enhanced by 30% when a strengthened circle is installed (Fig. 3*G*). In addition, judiciously patterning the strengthened regions can guide the crack to follow a wavy path, while the crack path in the virgin material is almost a straight line (Fig. 3*H*).

Photosynthesis can also be harnessed to strengthen 3D-printed structures. Similar to the treelike and Popeye-like structures in

Fig. 1 *C–F*, homogeneous light illumination can strengthen an Octet lattice to sustain a weight that is 830 times the lattice's own weight, without buckling the beams (*SI Appendix*, Fig. S27). In contrast, the unstrengthened lattice is significantly buckled by the same weight. This strengthening mechanism can further be used to fabricate lattices with a graded stiffness (Fig. 3 *I–M*). Creating materials with graded functional properties has been a long-standing challenge in 3D-printed materials, because grading properties requires continuously switching printing inks during fabrication (26). Here, we expose an initially homogenous Octet lattice to a light pattern with graded intensity, to impart a gradient in stiffness (Fig. 3*I* and *SI Appendix*, Fig. S28). This is because higher illumination doses lead to higher stiffness within a certain illumination dose range (Fig. 2*J*). The functionally graded lattice assumes a pale-yellow color at one end and remains green at the other end (Fig. 3*J* and *SI Appendix*, Fig. S29). We compare the results with two control samples, one stored in a dark environment for 8 h (fully soft, green lattice) and the other exposed to 4 h of homogeneous light illumination and 4-h darkness (fully stiffened, pale-yellow lattice). Indentation tests show that the effective Young's modulus of the graded lattice decreases from1.7 MPa at one end to 0.3 MPa at the other end (Fig. 3*K*). We apply a compressive load to the lattice with a relatively high loading rate (10 mm/s, Fig. 3*L*) and find that the absorbed energy in the graded lattice is around 1.7 times that of the soft lattice and 3.3 times that of the fully stiffened lattice (Fig. 3*M*).

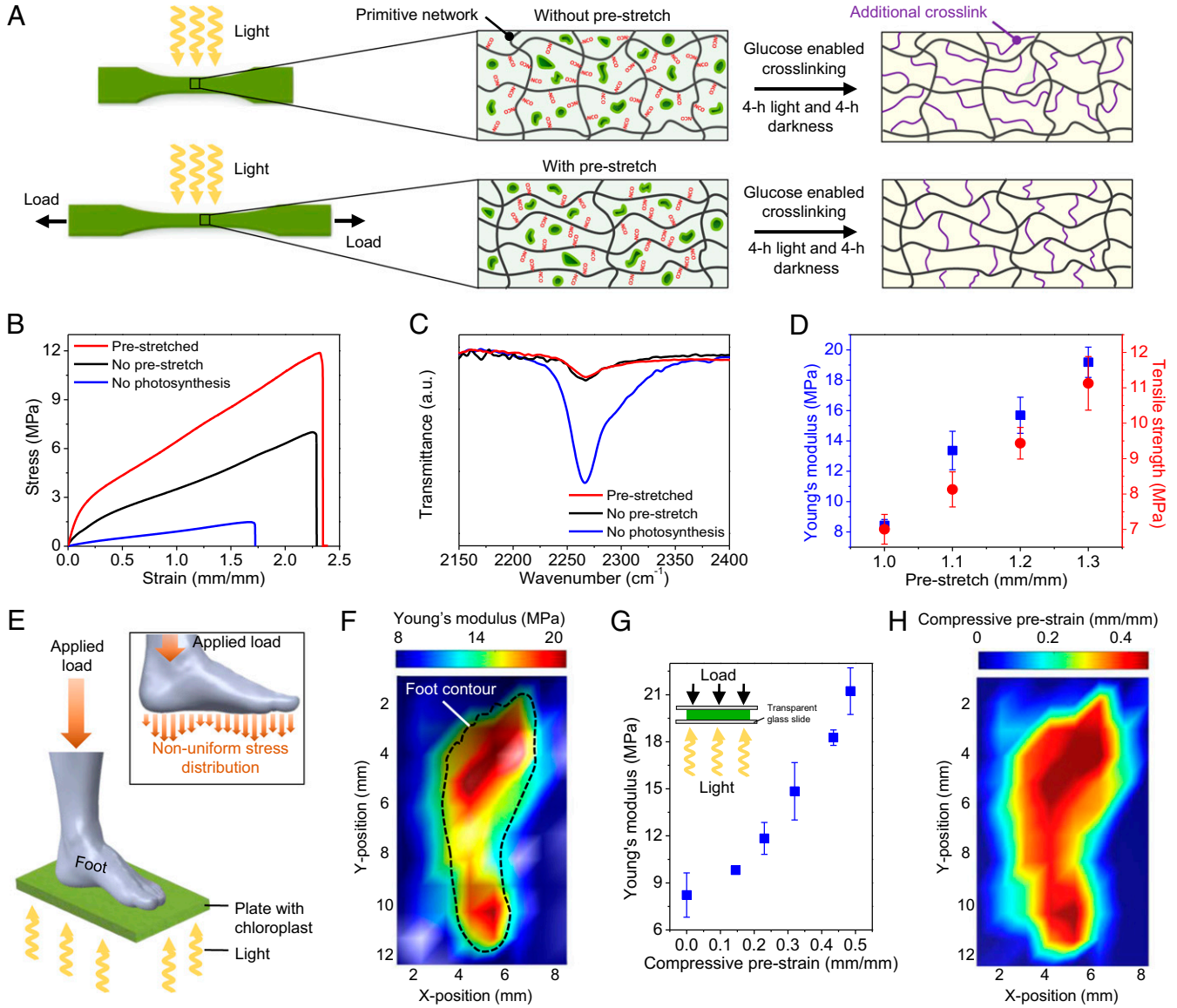

Fig. 4. Photosynthesis-assisted strengthening regulated by preloads. (*A*) Schematics to illustrate the photosynthesis-assisted strengthening in experimental samples without and with a prestretch. (*B*) Stress–strain curves of three samples: with a prestretch of 1.3 after 4-h light illumination and 4-h darkness, without a prestretch after 4-h light illumination and 4-h darkness, and without a prestretch after 8-h darkness. (*C*) FTIR spectra corresponding to the above three processed samples. (*D*) Young's moduli and tensile strengths of the processed samples with various prestretches. Error bars represent SDs of 3–5 samples. (*E*) Schematics to illustrate the photosynthesis process on a sample plate under nonuniform prestresses applied by a 3D-printed foot. (*F*) Young's modulus distribution of the processed sample plate. (*G*) The master curve between the applied compressive prestrain and the resultant Young's modulus of the sample after the photosynthesis process (4-h illumination and 4-h darkness). Error bars represent SDs of 3–5 samples. (*H*) The compressive prestrain distribution translated from the Young's modulus distribution in (*F*).

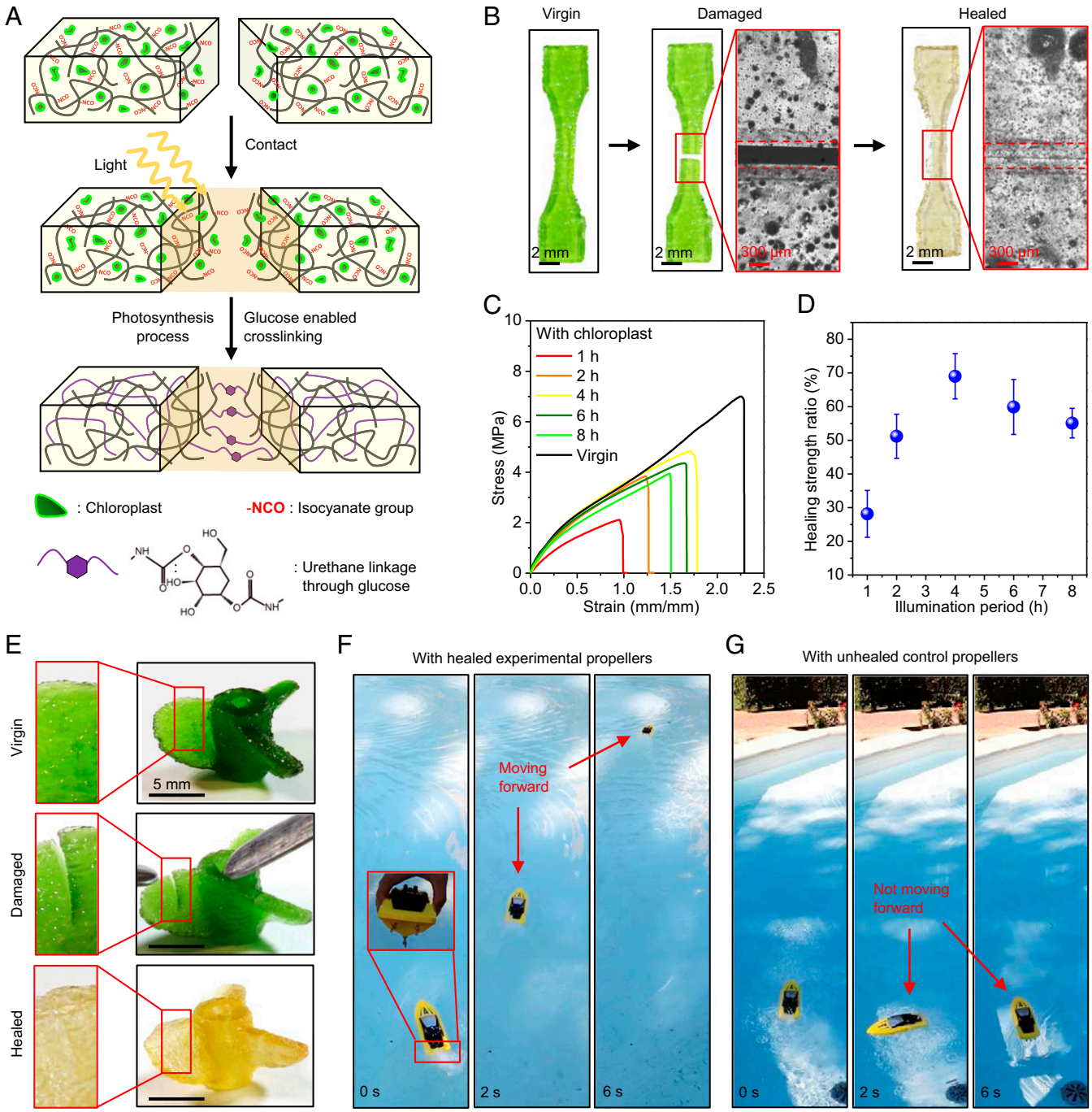

Fig. 5. Photosynthesis-assisted healing. (*A*) Schematic of photosynthesis-assisted healing of a fractured polymer through forming additional cross-links between free NCO groups and photosynthesis-produced glucose around the fracture surface. (*B*) Samples and interfacial microscope images at the virgin, damaged, and healed states. The healing process consists of 4-h light illumination and 4-h darkness. (*C*) Uniaxial tensile stress–strain curves of samples with various periods of light illumination time compared with that of the virgin sample. The virgin sample went through the photosynthesis process with 4-h light illumination and 4-h darkness. (*D*) Healing strength ratios of healed samples for various illumination periods. The healing strength ratio is defined as the tensile strength of the healed polymer normalized by that of the virgin sample. The error bars represent SDs of 3–5 samples. (*E*) Three-dimensional-printed experimental propeller structure at the virgin, damaged, and healed state. (*Insets*) Crack regions on a sector wing. (*F*) The healed experimental propellers assembled on a remotely controlled boat can facilitate the forward movement. (*G*) The unhealed propellers made of control 2 polymer ink (with free NCO groups but without chloroplasts) assembled on a remotely controlled boat cannot facilitate the forward movement.

Photosynthesis-Assisted Strengthening Regulated by Preloads

Mechanical loads can regulate plant remodeling through mechanotransduction pathways, to achieve higher stiffness and strength than those without the mechanical loads (5). Inspired by plants, we here show that the photosynthesis-assisted strengthening of the experimental polymer can be regulated by mechanical preloads (Fig. 4*A*). We apply a prestretch to a sample, followed by a photosynthesis process (4-h illumination and 4-h darkness). The processed sample with a prestretch of 1.3 shows

higher Young's modulus and tensile strength by factors of 228 and 159%, respectively, compared to those without a prestretch (Fig. 4*B*). The enhancement of Young's modulus and tensile strength is not due to the density increase of additional cross-links, because FTIR spectra reveal that the density of additional cross-links in the processed prestretched sample is almost the same as that without a prestretch (Fig. 4*C*). We hypothesize that the enhancement is probably attributed to the architecture change of the additional cross-links corresponding to the deformation of the primitive network (Fig. 4*A*), because the formation of additional cross-links is based on the side chains with NCO groups. Further experiments show that Young's moduli and tensile strengths of the processed samples increase with increasing prestretches (Fig. 4*D* and *SI Appendix*, Fig. S30). This mechanism can be harnessed to realize a nonuniform stiffness distribution with nonuniform prestresses. For example, we apply nonuniform prestresses on a sample plate with a 3D-printed foot, and then illuminate light to enable the photosynthesis process (Fig. 4*E*). Indentation tests reveal an inhomogeneous stiffness distribution on the sample (Fig. 4*F*). To translate the stiffness mapping to a prestrain mapping, we need to obtain a master curve between a homogeneous compressive prestrain on a sample disk and the resultant stiffness of the sample after the photosynthesis process (4-h illumination and 4-h darkness) (Fig. 4*G*). With such a master curve, a prestrain mapping (Fig. 4*H*) can be translated from the stiffness mapping in Fig. 4*F*. The demonstrated function may facilitate the design of future customized footwear by fabricating shoe soles with an inhomogeneous stiffness distribution that is corresponding to the inhomogeneous stress distribution applied by the foot.

Note that the postcuring of a partially cured photoresin can enhance the stiffness (27, 28). However, the mechanism of forming additional cross-links is drastically different from that in the current work, because the postcuring is based on the free monomers that are typically not connected to the primitive network (*SI Appendix*, Fig. S31*A*). Thus, the prestretch of the primitive network would have a negligible effect on the architecture of additional cross-links. Experiments show that prestretch can hardly regulate the stiffness and strength of the postcured polymer (*SI Appendix*, Fig. S31 *B–D*).

Photosynthesis-Assisted Healing

Some plants exhibit outstanding healing capability during grafting and wound repairing (29, 30). Inspired by plants, we here show that photosynthesis can assist the healing of a fractured polymer sample by forming additional cross-links between free NCO groups and photosynthesis-produced glucose at the fracture surfaces (Fig. 5*A*). To demonstrate the healing process, we 3D-print a dumbbell-shaped sample with free NCO groups and embedded chloroplasts, cut it into two parts, and then bring the two parts into contact (Fig. 5*B* and Movie S1). After 4-h illumination and 4-h darkness, the fractured sample is healed with a smooth healing interface, verified by a microscopic image around the interface (Fig. 5*B*). The healed sample can be stretched up to 1.8 times of original length without breaking (*SI Appendix*, Fig. S32 and Movie S1). To quantify the healing performance, we measure the tensile stress–strain behaviors of the healed samples after the photosynthesis process with different illumination periods (Fig. 5*C*). We find that the tensile strength ratio (tensile strength of the healed sample normalized by that of the virgin sample) increases with increasing illumination periods within 0–4 h and then decrease afterward (4–8 h) (Fig. 5*D*). The healing strength ratio for 4-h illumination can reach as high as 70 ± 7%. The decrease of the healing strength ratio after 4 h is probably because extralong illumination periods may degrade the chloroplasts, associated with the reduction of the exported glucose concentration (17, 18). As a contrast, the control 2 polymer with free NCO groups but without embedded chloroplasts exhibits a poor healing performance with the healing strength ratio as low as 9% (*SI Appendix*, Fig. S33*A*). The microscopic image shows that the contacted fracture interface still leaves an evident gap after 4-h illumination and 4-h darkness (*SI Appendix*, Fig. S33*B*).

The photosynthesis-assisted healing mechanism can be harnessed to repair a propeller 3D-printed with the experimental polymer ink (Fig. 5 *E–G*). A crack is installed on each wing of the propeller, and these cracks can be healed after the photosynthesis process (4-h illumination and 4-h darkness, Fig. 5*E*). On the contrary, cracks on the wings of a propeller 3D-printed with the control 2 polymer ink cannot be healed with the illumination process (*SI Appendix*, Fig. S34). To demonstrate the performance, the healed experimental propeller that assembled on a remotely controlled boat can facilitate the forward movement of the boat (Fig. 5*F* and Movie S2). However, the unhealed control propellers cannot push the boat forward due to the lack of enough propulsion force (Fig. 5*G* and Movie S2).

Conclusion

We harness photosynthesis in chloroplasts embedded in a synthetic polymer matrix to remodel 3D-printed structures and demonstrate matrix strengthening and crack healing. While the field of engineered photosynthesis shows a promising capability in producing energy fuels (31, 32), the current work extends the concept to advanced materials, by introducing a downstream reaction mechanism to use the photosynthesis-produced glucose. Besides, the presented photocurable polymers can be used in various photopolymerization-based 3D-printing systems, such as stereolithography (12, 13), polyjet (26), photopolymer waveguides (33), two-photon lithography (7, 34), continuous liquid production (35), and volumetric lithography (36, 37). To this end, the communication between living photosynthesis and synthetic 3D-printable polymers may open doors for hybrid synthetic-living materials with both complex architectures and biomimetic properties.

In the future study, maintaining the long-term living states of chloroplasts or even regenerating chloroplasts is a very important aspect. One possible solution would be refreshing of living chloroplasts using a flow system (38), such as a microfluidic flow of chloroplasts through a porous material framework.

Materials and Methods

Living chloroplasts were extracted from fresh baby spinach leaves (Spinacia oleracea L.). To fabricate polymer inks with free NCO groups, 0.02 mol of isophorone diisocyanate, 10 wt % of dimethylacetamide, and 1 wt % of dibutyltin dilaurate were mixed with the preheated Poly(tetrahydrofuran) (average molar mass 650 g/mol) at 70 °C and stirred with a magnetic stir bar for 1 h. After reducing the temperature to 40 °C, 0.01 mol of 2-Hydroxyethyl methacrylate was added and mixed for 1 h. Then, extracted chloroplasts (0–7 wt %) and 2 wt % of photoinitiator (phenylbis(2,4,6-trimethylbenzoyl)phosphine oxide) were gently mixed with the prepared polymer inks using a magnetic stir bar for 30 min at 5 °C in a dark environment. Subsequently, the polymer samples were 3D-printed with a bottom-up stereolithography system. Detailed descriptions of the experimental procedures and theoretical modeling are provided in *SI Appendix*.

Data Availability. All study data are included in the article and *SI Appendix*.

ACKNOWLEDGMENTS. Q.W. acknowledges the funding support from the Air Force Office of Scientific Research (Grant FA9550-18-1-0192, program manager: Dr. Ming-Jen Pan) and the NSF (Grants CMMI-1762567 and CMMI-1943598).

1. D. Barthélémy, Y. Caraglio, Plant architecture: A dynamic, multilevel and comprehensive approach to plant form, structure and ontogeny. *Ann. Bot.* **99**, 375–407 (2007).
2. Z. A. Popper *et al.*, Evolution and diversity of plant cell walls: From algae to flowering plants. *Annu. Rev. Plant Biol.* **62**, 567–590 (2011).
3. M. Ashby, "The CES EduPack database of natural and man-made materials" (Cambridge University and Granta Design, Cambridge, UK, 2008).
4. D. U. Shah, T. P. S. Reynolds, M. H. Ramage, The strength of plants: Theory and experimental methods to measure the mechanical properties of stems. *J. Exp. Bot.* **68**, 4497–4516 (2017).

5. A. Sampathkumar, A. Yan, P. Krupinski, E. M. Meyerowitz, Physical forces regulate plant development and morphogenesis. *Curr. Biol.* **24**, R475–R483 (2014).
6. R. L. Truby, J. A. Lewis, Printing soft matter in three dimensions. *Nature* **540**, 371–378 (2016).
7. J. Bauer *et al*., Nanolattices: An emerging class of mechanical metamaterials. *Adv. Mater.* **29**, 1701850 (2017).
8. Y. Yang *et al*., Recent progress in biomimetic additive manufacturing technology: From materials to functional structures. *Adv. Mater.* **30**, e1706539 (2018).
9. M. Kadic, G. W. Milton, M. van Hecke, M. Wegener, 3D metamaterials. *Nat. Rev. Phys.* **1**, 198–210 (2019).
10. J. U. Surjadi *et al*., Mechanical metamaterials and their engineering applications. *Adv. Eng. Mater.* **21**, 1800864 (2019).
11. D. Joly, R. Carpentier, "Rapid isolation of intact chloroplasts from spinach leaves" in *Photosynthesis Research Protocols*, R. Carpentier, Ed. (Humana Press, 2011), vol. 684, pp. 321–325.
12. Q. Wang *et al*., Lightweight mechanical metamaterials with tunable negative thermal expansion. *Phys. Rev. Lett.* **117**, 175901 (2016).
13. K. Yu *et al*., Healable, memorizable, and transformable lattice structures made of stiff polymers. *NPG Asia Mater.* **12**, 26 (2020).
14. J.-Y. Zhang *et al*., Synthesis, biodegradability, and biocompatibility of lysine diisocyanate-glucose polymers. *Tissue Eng.* **8**, 771–785 (2002).
15. A. L. B. Ramirez *et al*., Mechanochemical strengthening of a synthetic polymer in response to typically destructive shear forces. *Nat. Chem.* **5**, 757–761 (2013).
16. T. Matsuda, R. Kawakami, R. Namba, T. Nakajima, J. P. Gong, Mechanoresponsive self-growing hydrogels inspired by muscle training. *Science* **363**, 504–508 (2019).
17. D. W. Lawlor, *Photosynthesis: Molecular, Physiological and Environmental Processes* (Longman Scientific & Technical, 1993).
18. R. P. F. Gregory, *Biochemistry of Photosynthesis* (Wiley, London, 1977), vol. 5.
19. K. Okada, Y. Inoue, K. Satoh, S. Katoh, Effects of light on degradation of chlorophyll and proteins during senescence of detached rice leaves. *Plant Cell Physiol.* **33**, 1183–1191 (1992).
20. R. Rivlin, A. G. Thomas, Rupture of rubber. I. Characteristic energy for tearing. *J. Polym. Sci.* **10**, 291–318 (1953).
21. J.-Y. Sun *et al*., Highly stretchable and tough hydrogels. *Nature* **489**, 133–136 (2012).
22. H. Xiao, Z. H. Ping, J. W. Xie, T. Y. Yu, Permeation of CO2 through polyurethane. *J. Appl. Polym. Sci.* **40**, 1131–1139 (1990).
23. M. V. Korolevich, R. G. Zhbankov, V. V. Sivchik, Calculation of absorption-band frequencies and intensities in the IR-spectrum of alpha-d-glucose in a cluster. *J. Mol. Struct.* **220**, 301–313 (1990).
24. X. Liu, Y. Zhou, J. Xiao, F. Bao, Effects of chilling on the structure, function and development of chloroplasts. *Front. Plant Sci.* **9**, 1715 (2018).
25. J. D. Rawn, R. J. Ouellette, *Organic Chemistry: Structure, Mechanism, Synthesis* (Academic Press, 2018).
26. N. W. Bartlett *et al*., SOFT ROBOTICS. A 3D-printed, functionally graded soft robot powered by combustion. *Science* **349**, 161–165 (2015).
27. J. Rys, S. Steenhusen, C. Schumacher, C. Cronauer, C. Daraio, Locally addressable material properties in 3D micro-architectures. *Extreme Mech. Lett.* **28**, 31–36 (2019).
28. H. Yin, Y. Ding, Y. Zhai, W. Tan, X. Yin, Orthogonal programming of heterogeneous micro-mechano-environments and geometries in three-dimensional bio-stereolithography. *Nat. Commun.* **9**, 4096 (2018).
29. C. W. Melnyk, E. M. Meyerowitz, Plant grafting. *Curr. Biol.* **25**, R183–R188 (2015).
30. R. Bloch, Wound healing in higher plants. II. *Bot. Rev.* **18**, 655 (1952).
31. N. Kornienko, J. Z. Zhang, K. K. Sakimoto, P. Yang, E. Reisner, Interfacing nature's catalytic machinery with synthetic materials for semi-artificial photosynthesis. *Nat. Nanotechnol.* **13**, 890–899 (2018).
32. K. K. Sakimoto, N. Kornienko, P. Yang, Cyborgian material design for solar fuel production: The emerging photosynthetic biohybrid systems. *Acc. Chem. Res.* **50**, 476–481 (2017).
33. T. A. Schaedler *et al*., Ultralight metallic microlattices. *Science* **334**, 962–965 (2011).
34. L. R. Meza, S. Das, J. R. Greer, Strong, lightweight, and recoverable three-dimensional ceramic nanolattices. *Science* **345**, 1322–1326 (2014).
35. J. R. Tumbleston *et al*., Additive manufacturing. Continuous liquid interface production of 3D objects. *Science* **347**, 1349–1352 (2015).
36. M. Shusteff *et al*., One-step volumetric additive manufacturing of complex polymer structures. *Sci. Adv.* **3**, eaao5496 (2017).
37. B. E. Kelly *et al*., Volumetric additive manufacturing via tomographic reconstruction. *Science* **363**, 1075–1079 (2019).
38. T. E. Miller *et al*., Light-powered CO_2 fixation in a chloroplast mimic with natural and synthetic parts. *Science* **368**, 649–654 (2020).

Supplementary Information for

Photosynthesis Assisted Remodeling of Three-Dimensional Printed Structures

Kunhao Yu[1†], Zhangzhengrong Feng[1†], Haixu Du[1], An Xin[1], Kyung Hoon Lee[1], Ketian Li[1], Yipin Su[1], Qiming Wang[1*], Nicholas X. Fang[2*], Chiara Daraio[3*]

[1]Sonny Astani Department of Civil and Environmental Engineering, University of Southern California, Los Angeles, California 90089, United States.

[2]Department of Mechanical Engineering, Massachusetts Institute of Technology, Cambridge, Massachusetts 02139, United States.

[3]Division of Engineering and Applied Science, California Institute of Technology, Pasadena, California 91125, United States.

† Contribute equally.

*Correspondence to: qimingw@usc.edu (Q. Wang); nicfang@mit.edu (N. X. Fang); daraio@caltech.edu (C. Daraio).

This PDF file includes:

Other Supplementary Information for this manuscript include the following:

Materials and Methods

Materials. Poly(tetrahydrofuran) (PolyTHF, average molar mass 650 g/mol), isophorone diisocyanate (IPDI), dimethylacetamide (DMAc), 2-Hydroxyethyl methacrylate (HEMA), dibutyltin dilaurate (DBTDL), 1,6-hexanediol diacrylate (HDDA), α-D-Glucose, phenylbis(2,4,6-trimethylbenzoyl)phosphine oxide (photoinitiator), Sudan I (photoabsorber), HEPES buffer solution, Poly (ethylene glycol), Potassium phosphate tribasic (K_3PO_4), Magnesium chloride ($MgCl_2$), Sodium hydroxide (NaOH), Percoll (pH 8.5-9.5), and periodic acid (HIO_4) were purchased from Sigma-Aldrich and used without further purification. Baby spinach leaves (Spinacia oleracea L.) were purchased from Trader Joe's.

Extraction of chloroplasts. The HEPES buffer solution was prepared by mixing HEPES buffer (30×10^{-3}M, pH 5.0-6.0), poly(ethylene glycol) ($Mw. 8000, 10\%$ (w/v)), $M_g Cl_2$ $(2.5 \times 10^{-3}\ M)$, $K_3 PO_4$ $(0.5 \times 10^{-3}\ M)$, and DI Water. The HEPES buffer solution was then magnetically stirred for 3 h. NaOH solution was added to adjust the pH value to be around 7.6. The HEPES buffer solution was then stored in the fridge at 4°C for 3 h before use. Then, the fresh baby spinach leaves (Spinacia oleracea L.) were washed with DI water and then dried to remove the surface water. Next, the middle veins of the leaves were removed to obtain 65 g leaf meat from about 100 g of fresh leaves. Then, the leaf meat was ground with 100 ml HEPES buffer solution in the pre-chilled kitchen blender for about 2 minutes until the mixture became homogeneous. The mixture was centrifuged with 4000 RPM for 15 min at 4 °C (Eppendorf 5804R). Then, the supernatant was removed, and the chloroplast pellet was re-suspended in the HEPES buffer solution. After adding the suspended mixture on the top of 5 mL of 40% Percoll in two pre-chilled tubes, we centrifuged the mixture at 3636 RPM for 8 min at 4 °C. Later, we removed the supernatant and kept the pellet. Next, we washed the pellet by adding 10 mL HEPES buffer solution and piped it out twice to remove Percoll. Before using the extracted chloroplast, we put the tubes upside down in the fridge for 1 h to get rid of the remained water or buffer solution from the chloroplast pellet.

Preparation of polymer inks with and without free NCO groups. To fabricate polymer inks with free NCO groups (**Fig. S1**), we preheated 0.01 mole of PolyTHF at 100℃ and exposed to Nitrogen environment for 1 h to remove moisture and oxygen. 0.02 mole of IPDI, 10 wt% of DMAc and 1 wt% of DBTDL were mixed with the preheated PolyTHF at 70℃ and stirred with a magnetic stir bar for 1 h. After reducing the temperature to 40℃, 0.01 mole of HEMA was added and mixed for 1 h to complete the synthesis. To fabricate polymer inks without free NCO groups (**Fig. S12**), we used a similar procedure as that of the polymer ink with free NCO groups except for 0.02 mole of HEMA in the last step. For the additive manufacturing, 2 wt% of photoinitiator (phenylbis(2,4,6-trimethylbenzoyl)phosphine oxide) was mixed with the polymer inks and stored in a dark amber glass bottle until use.

Preparation of polymer inks with chloroplasts. Extracted chloroplasts of various weight percent from 0 wt% to 7 wt% were gently mixed with the prepared polymer inks (with or without free NCO groups) using a magnetic stir bar for 30 min at 5℃ in a dark environment to prevent the degradation of chloroplasts (**Fig. S2**).

3D printing process. A similar printing technique was described elsewhere (**Fig. S3**) [12,13]. A computer-aided design (CAD) model was designed and converted into an STL file, which was then sliced into an image sequence. The sliced images were then used to print the 3D

structure with a bottom-up stereolithography (SLA) printer. An image-patterned light with a wavelength of 405 nm was projected from the bottom to a resin bath that was filled with a synthesized polymer ink. A motor-controlled printing stage was mounted onto the resin bath with a prescribed liquid height. The light-exposed resin was solidified and bonded onto the printing stage. As the printing stage was lifted, the fresh resin refluxed beneath the printing stage. By lowering the printing stage at prescribed height and illuminating the resin with another slice image, a second layer was printed and bonded onto the first layer. These processes were repeated to form a 3D-architected structure. A Teflon membrane with low surface tension (~20 mN/m) was employed to reduce the separation force between the solidified part and the printing window.

Photosynthesis process in different conditions. The 3D-printed solid samples were placed in a white-light chamber (CL-1000 Ultraviolet Crosslinker with five UVP 34-0056-01 bulbs, light intensity 69.3 W/m^2) with different exposure conditions. For the experimental group and control 2 group in **Figs. 2A** and **2C**, the samples went through 4-h illumination of white light followed by 4-h darkness in the chamber. For the control 1 group in **Fig. 2B**, the samples went through 8-h darkness in the chamber. For the samples with chloroplasts of various weight concentrations (0-7 wt%, **Fig. 2I)**, they went through 4-h light illumination and 4-h darkness. For the samples with various light-illumination periods (**Fig. 2J)**, they went through periods of light illumination and darkness of the same length. For example, the 15-minutes group went through 15-minute light illumination and 15-minute darkness.

Characterization of strengthening effect. Dumbbell-like samples were fabricated with the aforementioned 3D-printing process (length 5 mm, width 2 mm, and thickness 2 mm shown in **Fig. S9A**). After the respective photosynthesis or non-photosynthesis processes described above, the samples were placed in a dark chamber (40℃) for 12 h to evaporate the residual solvent. Then, the samples were uniaxially stretched until rupture with a strain rate of 0.05 s^{-1} using a mechanical tester (Instron, model 5942). Spectrum TWO FT-IR Spectrometer (PerkinElmer, USA) was used for the FT-IR analyses before and after the respective photosynthesis or non-photosynthesis processes with the scanning range of 450 to 4000 cm^{-1} at a resolution of 0.5 cm^{-1}.

The fracture energies of the polymers after different photosynthesis conditions were measured by using pure-shear fracture tests [20,21]. Unnotched and notched samples (length $a_0 = 40mm$, thickness $b_0 = 1mm$ and distance between two clamps $L_0 = 5mm$) were employed (**Figs. S9B, S11**). The notched sample was prepared by using a razor blade to cut a 20-mm notch in the middle left region. Both samples were uniaxially stretched with a strain rate of 0.05 s^{-1} until rupture. A camera was used to record the critical distance (denoted as L_c) between the clamps when the crack starts propagating on the notched sample. The fracture energy was calculated as $U(L_c)/(a_0 b_0)$, where $U(L_c)$ is the work done by the applied force before the critical distance, illustrated as the area beneath the force-distance curve in the unnotched test **(Fig. S11)**.

Verification of glucose production from the embedded chloroplasts. The prepared polymer ink without free NCO groups (**Fig. S12**) was gently mixed with 5wt% of extracted chloroplasts with a magnetic stir bar for 30 min at 5℃ in a dark environment to prevent the degradation of chloroplasts. The mixture was 3D-printed into dumbbell-like samples. The prepared samples were placed in a white-light chamber (light intensity 69.3 W/m^2) for two different conditions, including 4-h light illumination and 4-h darkness, and 8-h darkness. The

FTIR analyses were conducted to monitor the transmittance corresponding to the OH groups in the polymer samples at the as-fabricated state, after 4-h light and 4-h darkness, and after 8-h darkness (**Figs. S13AB**). After removing the residual solvent in a dark chamber (40℃) for 12 h, the samples were then uniaxially stretched until rupture with a strain rate of 0.05 s^{-1} (**Fig. S13D**).

Characterization of polymer strengthened by glucose. α-D-glucose was first mixed with polymer ink with free NCO groups to make different glucose concentrations (0 M-0.389 M). The mixture was 3D-printed into dumbbell-like samples. The FTIR analyses were conducted to monitor the transmittance corresponding to the NCO groups in the polymer samples with different glucose concentrations. After removing the residual solvent in a dark chamber (40℃) for 12 h, the samples were then uniaxially stretched until rupture with a strain rate of 0.05 s^{-1}.

Effects of chloroplast concentration and illumination time. The fabricated polymer samples with free NCO groups and chloroplasts of various weight concentrations (0-7wt%) were uniaxially stretched until rupture with a strain rate of 0.05 s^{-1} after 4-h light illumination and 4-h darkness. The fabricated polymer samples with free NCO groups and 5 wt% chloroplasts after undergoing various light illumination periods (0-6 h) and the respective darkness periods (same length of the illumination period), were also uniaxially stretched until rupture with a strain rate of 0.05 s^{-1}. The Young's modulus and tensile strength of each sample were calculated from the obtained tensile stress-strain curve.

Freezing chloroplasts with a chilling temperature. The fabricated polymer samples with free NCO groups and 5 wt% chloroplasts were first sealed in a petri dish and then immersed in an ice bath. The samples with the temperature of 0-4℃ underwent 2-h light illumination and 2-h darkness. These samples were divided into two parts. Some processed samples were uniaxially stretched until rupture with a strain rate of 0.05 s^{-1}. For other processed samples, the temperature was first raised to room temperature (25℃); and then these samples underwent another 2-h light illumination and 2-h darkness, followed by being uniaxially stretched until rupture with a strain rate of 0.05 s^{-1}.

Cleavage of glucose crosslinkers in the strengthened polymer. The strengthened polymer samples were immersed in a 2 M periodic acid solution (2 moles of periodic acid and 1 L of DMAc) for 6 h. The samples were swollen by around 220% and then de-swollen by evaporating the residual solvent in a dark chamber (40℃) for 12 h. For the control group, the strengthened samples were immersed in the DMAc solvent for 6 h and then de-swollen by evaporating the solvent in a dark chamber (40℃) for 12 h. Both sets of samples were then uniaxially stretched until rupture with a strain rate of 0.05 s^{-1}.

Local strengthening with an "S" shape. Plate samples (with free NCO groups and 5 wt% embedded chloroplasts) with a size of 14mm × 10mm × 2mm were fabricated by the aforementioned 3D-printing system (**Fig. 3B**). The samples were then placed in an amber container, covered with a mask with an "S" shape, and put in the white-light chamber for 4-h illumination and 4-h darkness. Young's modulus distribution over the sample surface was measured by using a round-flat end cylinder indenter with radius R=0.5 mm loaded on the Instron mechanical tester to indent the sample by applying force F to certain indentation depth δ. The Young's modulus of each location was calculated as $E = F(1-\upsilon^2)/(2R\delta)$, where $\upsilon =$

0.48 is the Poisson's ratio of material (**SI appendix, Fig. S26**). The Young's modulus distribution map was plot using MATLAB (**Fig. 3C**).

Local strengthening with circles. Plate samples (with free NCO groups and 5 wt% embedded chloroplasts) with sizes of 20 mm × 20 mm × 2 mm (for **Fig. 3E**) and 56 mm × 20 mm × 2 mm (for **Fig. 3H**) were fabricated by the aforementioned 3D-printing system. The 20 mm × 20 mm × 2 mm sample was locally strengthened with a circular-shaped mask (circle diameter = 3 mm) next to a 3-mm edge notch. The 56 mm × 20 mm × 2 mm sample was locally strengthened with 18 circular patterns (circle diameter = 1mm) with a certain path next to an edge notch. Both samples were then clamped at the left two corners for the tearing test with the Instron mechanical tester.

Homogeneous and graded lattice structures. Lattice structures (with free NCO groups and 5 wt% embedded chloroplasts) with various units (2 × 2 × 1 for **Fig. S27** and 10 × 4 × 1 for **Fig. 3J**) were fabricated by the aforementioned 3D-printing system. For the structures with homogeneous light, the printed samples were placed in the white-light chamber with 2-h illumination on the front side and 2-h illumination on the rear side, followed with 4 h darkness. For the structure with the darkness condition, the printed samples were placed in the dark chamber for 8 h. For the structures treated with a graded light, a transparent cover was attached with different layers of vinyl-coated white tape and covered on top of the printed sample (**Fig. S28**). The entire setup was then placed in the white-light chamber to induce a graded light intensity varies from 0 to 69.3 W/m^2 on the long edge direction of the sample for each unit distance (2 mm). The samples were placed in the graded light chamber with 2-h illumination on the front side and 2-h illumination on the rear side, followed with 4 h darkness.

The 2 × 2 × 1 lattice structures with different conditions were tested under a compressive load along the longitudinal direction (gradient direction) with a strain rate of 0.05 s^{-1} using the Instron mechanical tester (**Fig. S27**). The Young's modulus of each unit of the 10 × 4 × 1 lattice structures was tested lattice by the indentation test. The Young's modulus can be calculated as $E = F(1-\upsilon^2)/(2R\delta)$, where F is the applied load, $\upsilon = 0.48$ is the effective Poisson's ratio, R is the radius of a round-flat end cylinder indenter (R=1 mm), and δ is the indentation depth.

The energy absorption behaviors of the 10 × 4 × 1 lattices were characterized by impact loading tests with a relatively large strain rate of 10 mm/s. The absorbed energy was calculated by the area underneath the load-displacement curves (**Fig. 3L**).

3D-printing and strengthening of tree-like structures. The tree-like structures were fabricated by the aforementioned 3D printing system using the polymer ink with free NCO groups and 5 wt% embedded chloroplast. The printed tree-like structures were then placed in a white-light chamber with 2-h light illumination (light intensity 69.3 W/m^2) and 2-h darkness. To characterize the load sustaining capability of the tree-like structures in different states, we hang a 1-g metal ring on one tree branch at the unstrengthened state (with 4-h darkness) and after photosynthesis process (2-h illumination and 2-h darkness).

3D-printing and strengthening of Popeye-like structures. The Popeye-like structures (height 23 mm, width 15 mm, and depth 5 mm) were fabricated by the aforementioned 3D printing system using the polymer ink with free NCO groups and 5 wt% embedded chloroplast. The printed Popeye-like structures were then placed in a white-light chamber with 2-h light illumination (light intensity 69.3 W/m^2) and 2-h darkness. To characterize the weight sustaining

capability of the Popeye-like structures in different states, we loaded a 200-g weight (two weights of 100 g each) on a glass slide that was placed on the strengthened or unstrengthened Popeye-like structures.

Effect of pre-stretch on Photosynthesis-assisted strengthening. The fabricated polymer samples with free NCO groups and 5 wt% chloroplasts were first uniaxially pre-stretched with various stretches ($\lambda = 1 - 1.3$) and undergone 4-h light illumination and 4-h darkness. Then, the processed samples were then cut into smaller samples with a dumbbell-like shape, which were uniaxially stretched until rupture with a strain rate of 0.05 s^{-1}. The FTIR analyses were conducted to monitor the transmittance corresponding to the NCO groups in the polymer samples with different pre-stretches.

Photosynthesis-assisted strengthening under a non-uniform pre-stress distribution. Plate sample (with free NCO groups and 5 wt% embedded chloroplasts) with a size of 12 mm × 8 mm × 2 mm was fabricated by the aforementioned 3D-printing system. A foot-like 3D structure with non-uniform surface was also 3D-printed with a rigid polymer ink (HDDA). The foot-like structure was compressed on the sample plate by deforming 1 mm in depth. The deformation-induced a non-uniform stress-distribution on the sample plate. With the deformation, the plate illuminated by white light (light intensity 69.3 W/m^2) from the bottom for 4 h, followed by 4-h darkness. Young's modulus distribution over the sample surface was measured by using a round-flat end cylinder indenter with radius R=0.5 mm loaded on the Instron mechanical tester (**Fig. S26**).

Characterization of Photosynthesis-assisted healing. 3D printed dumbbell-shaped samples with free NCO groups and 5wt% embedded chloroplasts were first cut into two parts with a razor blade, and the fractured surfaces were brought into contact immediately. The samples were then placed in a white-light chamber with light illuminating time various from 1 h to 8 h, followed by the darkness with the same respective period. For the control, 3D printed dumbbell-shaped samples with free NCO groups but without embedded chloroplasts were used. Both healed and control samples were uniaxially stretched to rupture with the same strain rate (0.05 s^{-1}). An optical microscope (Nikon Eclipse LV100ND) was used to image the healing region (**Fig. 5B**).

Photosynthesis-assisted healing of 3D-printed propeller. The 3D-printed propellers were fabricated by the aforementioned 3D printing system. The experiment propellers were fabricated using polymer inks with free NCO groups and 5wt% embedded chloroplasts. 4-mm damages were introduced on each sector of the printed propellers with a razor blade. The fractured surfaces were aligned into contact immediately and then placed in a white-light chamber with 4-h light illumination and 4-h darkness. Two healed propellers were assembled onto a remotely controlled boat to provide the pushing force to move forward in a pound (**Fig. 5F**). The control propellers were fabricated using polymer inks with free NCO groups but without chloroplasts. The controlled propellers were also damaged, healed, and assembled onto the remotely controlled boat (**Fig. 5G**).

Supplementary analysis

Mathematical model of polymer strengthening by additional crosslinking

In the current work, the polymer ink is first crosslinked by the photo-initiated addition reaction of the acrylate groups (**Fig. S2**). Within this primary polymer network, NCO groups are active sites that can have a strong reaction with hydroxyl groups (OH) on the chloroplast-produced glucose to form urethane linkages (-NH-CO-O-). Since a glucose molecule has multiple OH groups, it is hypothesized that the OH groups on the chloroplast-produced glucose can bridge multiple NCO groups to create new crosslinks additional to the acrylate-enabled crosslinks within the designed polymer matrix (**Fig. S17A**).

(1) Before strengthening

Before strengthening, the polymer network is assumed to feature a homogenous chain length. The chain length is described by the Kuhn length, denoted as N_0 and chain number per unit volume as n_0. The strain energy density of the polymer network can be written as [1,2]

$$W_0 = n_0 k_B T N_0 \left(\frac{\beta_0}{tanh\beta_0} + ln\frac{\beta_0}{sinh\beta_0}\right) \tag{S1}$$

where k_B is the Boltzmann constant, T is the temperature in Kelvin, and

$$\beta_0 = L^{-1}\left(\frac{\Lambda}{\sqrt{N_0}}\right) \tag{S2}$$

where $L^{-1}(\ \ )$ is the inverse Langevin function and Λ is the chain stretch. Here, we follow an affine deformation assumption that the microscopic polymer chain deformation affinely follows the macroscopic deformation in three principal directions; thus, the chain stretch can be expressed as

$$\Lambda = \sqrt{\lambda_1^2 + \lambda_2^2 + \lambda_3^2} \tag{S3}$$

This affine deformation assumption has been widely adopted for deriving the constitutive models for rubber-like materials, such as the New-Hookean model [1] and the Arruda-Boyce model [2]. The chain stretch expressed in Eq. S3 is directly adopted from the New-Hookean model [1,3].

If the polymer is incompressible, the Cauchy stresses in three principal directions can be written as

$$\begin{cases} \sigma_1 = \lambda_1 \frac{\partial W_0}{\partial \lambda_1} - P \\ \sigma_2 = \lambda_2 \frac{\partial W_0}{\partial \lambda_2} - P \\ \sigma_3 = \lambda_3 \frac{\partial W_0}{\partial \lambda_3} - P \end{cases} \tag{S4}$$

where P is the hydrostatic pressure. Under uniaxial tension with $\lambda_1 = \lambda$ and $\lambda_2 = \lambda_3 = \lambda^{-1/2}$, the Cauchy stresses σ_2 and σ_3 vanish. The Cauchy stress σ_1 can be formulated as

$$\sigma_1 = \lambda_1 \frac{\partial W_0}{\partial \lambda_1} - \lambda_2 \frac{\partial W_0}{\partial \lambda_2} \tag{S5}$$

The corresponding tensile nominal stress (engineering stress) can be calculated as

$$s_1 = \frac{\sigma_1}{\lambda_1} = n_0 k_B T \sqrt{N_0} \frac{\lambda - \lambda^{-2}}{\sqrt{\lambda^2 + 2\lambda^{-1}}} L^{-1}\left(\sqrt{\frac{\lambda^2 + 2\lambda^{-1}}{N_0}}\right) \quad \text{(S6)}$$

Equation S6 can be used to explain the stress-strain behaviors of polymer samples before strengthening. Only two fitting parameters (polymer chain length N_0 and chain number density n_0) are required.

(2) Strengthening by forming additional crosslinks

Once the glucose is introduced, additional crosslinks form through the reactions between the free NCO groups and the OH groups on the glucose (**Fig. S17A**). One glucose molecule with 5 OH groups is only required to bridge two NCO groups to form a crosslink. Thus, one glucose molecule is able to at most form 2.5 crosslinks within the network. The number of the introduced glucose molecules per unit volume is denoted as n_g and the formed additional crosslink number per unit volume is denoted as n_a, which should follow $n_g \leq n_a \leq 2.5 n_g$.

As shown in **Fig. S17B**, two polymer chains with chain length N_0 become four polymer chains with shorter lengths after introducing an additional crosslink. In a general case, these four polymer chains may have different chain lengths. Here, to capture the essential physics with a simple mathematic formulation, we assume these four polymer chains have the same chain length, as $N_0/2$. In a more general case shown in **Fig. S17C**, we assume the crosslink formed between a chain with a length of $N_0/2^i$ and a chain with a length of $N_0/2^j$ induces four chains with respective half lengths, where $i = 0,1,2\cdots$ and $j = 0,1,2\cdots$.

After introducing n_a additional crosslinks per unit volume, the initially homogeneous chain length (N_0) will become inhomogeneous, with a chain length distribution over lengths of N_0, $N_0/2$, …., and $N_0/2^m$, where $m \geq 1$. The value of m is constrained by choosing the largest m to ensure

$$\frac{N_0}{2^m} \geq N_{min} \quad \text{(S7)}$$

where N_{min} is the admissible smallest chain length.

To estimate the chain number of each type of chain length per unit volume, we treat the additional crosslinking process as m steps. In each step, additional crosslinks of a certain amount are introduced. We employ two methods:

Method 1: Equal number of incremental crosslinks

In method 1, we assume that probabilities of forming a crosslink on the chain with a length of $N_0/2^i$ and the chain with a length of $N_0/2^j$ are equal, where $i = 0,1,2\cdots$ and $j = 0,1,2\cdots$. Under this assumption, the incremental additional crosslinking density for each step is equal, denoted as dn_a:

$$dn_a = \frac{n_a}{m} \quad \text{(S8)}$$

In the following, we will go through each step to calculate the volume density of polymer chains with length $N_0/2^j$, where $j = 0,1,2\cdots$. We denote it as C_j, where $j = 0,1,2\cdots$.

In step 1, some of the initial chains with length N_0 become shorter chains with a length of $N_0/2$ after adding dn_a crosslinks if $2dn_a \le n_0$. At the end of step 1, we have:

$$C_0 = n_0 - 2dn_a \tag{S9a}$$

$$C_1 = 4dn_a \tag{S9b}$$

In step 2, three possible routes to form crosslinks: between two chains with the length of N_0, between two chains with the length of $N_0/2$, and between a chain with the length of N_0 and a chain with the length of $N_0/2$. The probabilities for partitioning chains with length N_0 and chains with length $N_0/2$ are equal. Therefore, at the end of step 2, we have:

$$C_0 = n_0 - 2dn_a - 2(dn_a/2) \tag{S10a}$$

$$C_1 = 4dn_a + 4(dn_a/2) - 2(dn_a/2) \tag{S10b}$$

$$C_2 = 4(dn_a/2) \tag{S10c}$$

Similarly, at the end of step 3, we have:

$$C_0 = n_0 - 2dn_a - 2(dn_a/2) - 2(dn_a/3) \tag{S11a}$$

$$C_1 = 4dn_a + 4(dn_a/2) - 2(dn_a/2) + 4(dn_a/3) - 2(dn_a/3) \tag{S11b}$$

$$C_2 = 4(dn_a/2) + 4(dn_a/3) - 2(dn_a/3) \tag{S11c}$$

$$C_3 = 4(dn_a/3) \tag{S11d}$$

Eventually, at the end of step *m*, we have:

$$C_0 = n_0 - 2dn_a\left(1 + \tfrac{1}{2} + \tfrac{1}{3} + \cdots + \tfrac{1}{m}\right) \tag{S12a}$$

$$C_1 = 2dn_a + 2dn_a\left(1 + \tfrac{1}{2} + \tfrac{1}{3} + \cdots + \tfrac{1}{m}\right) \tag{S12b}$$

$$C_2 = 2(\tfrac{dn_a}{2}) + 2dn_a\left(\tfrac{1}{2} + \tfrac{1}{3} + \cdots + \tfrac{1}{m}\right) \tag{S12c}$$

……

$$C_j = 2(dn_a/j) + 2dn_a\left(\tfrac{1}{j} + \tfrac{1}{j+1} + \cdots + \tfrac{1}{m}\right) \tag{S12d}$$

……

$$C_m = 4(dn_a/m) \tag{S12e}$$

The volume density of chains with length $N_0/2^j$ at the end of step *m* can be summarized as

$$C_j = \begin{cases} n_0 - \frac{2n_a}{m}\left(1 + \frac{1}{2} + \frac{1}{3} + \cdots + \frac{1}{m}\right), j = 0 \\ \frac{2n_a}{m}\left(\frac{2}{j} + \frac{1}{j+1} + \cdots + \frac{1}{m}\right), 1 \le j \le m-1 \\ \frac{4n_a}{m^2}, j = m \end{cases} \tag{S13}$$

After strengthening, the polymer chain length is inhomogeneous with a chain length distribution over lengths of N_0, $N_0/2$, …., and $N_0/2^m$, where $m \geq 1$. The chain length distribution is shown in Eq. S13. We assume that under deformation, each polymer chain deform following an affine deformation assumption that the microscopic polymer chain deformation affinely follows the macroscopic deformation in three principal directions; thus, the chain stretch of the chain with the length of $N_0/2^j$ ($j = 0,1,2\cdots$) can be expressed as [4-10]

$$\Lambda_j = \sqrt{\lambda_1^2 + \lambda_2^2 + \lambda_3^2} \tag{S14}$$

The strain energy of the whole polymer network per unit volume can be formulated as [4-10]

$$W_s = \sum_{j=0}^{m} \left[C_j k_B T \left(\frac{N_0}{2^j}\right) \left(\frac{\beta_j}{tanh\beta_j} + ln\frac{\beta_j}{sinh\beta_j}\right)\right] \tag{S15}$$

$$\beta_j = L^{-1}\left(\frac{\Lambda_j}{\sqrt{N_0/2^j}}\right) \tag{S16}$$

where the chain stretch Λ_j is given in Eq. S14. Under uniaxial tension with $\lambda_1 = \lambda$ and $\lambda_2 = \lambda_3 = \lambda^{-1/2}$, the nominal tensile stress of the incompressible polymer after strengthening can be calculated as

$$s_{s1} = \sum_{j=0}^{m} \left[C_j k_B T \sqrt{N_0/2^j} \frac{\lambda - \lambda^{-2}}{\sqrt{\lambda^2 + 2\lambda^{-1}}} L^{-1}\left(\sqrt{\frac{\lambda^2 + 2\lambda^{-1}}{N_0/2^j}}\right)\right] \tag{S17}$$

In method 1, there is a requirement for the relationship between n_a and m. For example, if $m = 1$, the maximal possible crosslinking point density is $n_0/2$. This condition is to ensure the chain density of chains with length N_0 is not negative. For a certain $m \geq 1$, the requirement of the possible crosslink density is

$$(m-1)/\left[2\left(1 + \frac{1}{2} + \frac{1}{3} + \cdots + \frac{1}{m-1}\right)\right] < n_a/n_0 \leq m/\left[2\left(1 + \frac{1}{2} + \frac{1}{3} + \cdots + \frac{1}{m}\right)\right] \tag{S18}$$

Method 2: Unequal number of incremental crosslinks

In method 2, we assume that the probability of forming a crosslink on the chain with the length of $N_0/2^i$ is higher than that of forming a crosslink on the chain with the length of $N_0/2^j$ when $i < j$. In an extreme case, the crosslink occurs first on the chain with the length of $N_0/2^i$, and then on the chain with the length of $N_0/2^{i+1}$. In other words, the crosslinking reaction on the longer chains always happens before the crosslinking reaction on the shorter chains. Following the assumption, we can naturally define the *i*th step as the step with the occurrence of the crosslinking reaction on the chain with the length of $N_0/2^{i-1}$. The process will move to the next step only when there are enough crosslinkers to consume all the chains with the length of $N_0/2^{i-1}$.

If the crosslinking reaction stops at step 1, there are only two types of chains: chains with length N_0 and $N_0/2$. Their volume densities can be calculated as

$$C_0 = n_0 - 2n_a \tag{S19a}$$

$$C_1 = 4n_a \tag{S19b}$$

The requirement is $0 < n_a/n_0 \leq 1/2$.

If the crosslinking reaction stops at step 2, there are only two types of chains: chains with length $N_0/2$ and $N_0/2^2$. Their volume densities can be calculated as

$$C_1 = 2n_0 - 2\left(n_a - \frac{n_0}{2}\right) = 3n_0 - 2n_a \tag{S20a}$$

$$C_2 = 4\left(n_a - \frac{n_0}{2}\right) \tag{S20b}$$

The requirement is $1/2 < n_a/n_0 \leq 3/2$.

If the crosslinking reaction stops at step m, at the end of step m, there are only two types of chains: chains with lengths $N_0/2^{m-1}$ and $N_0/2^{m-1}$. Their volume densities can be calculated as

$$C_{m-1} = 2^{m-1}n_0 - 2\left[n_a - \left(2^{m-2} - \frac{1}{2}\right)n_0\right] = (2^m - 1)n_0 - 2n_a \tag{S21a}$$

$$C_m = 4\left[n_a - \left(2^{m-2} - \frac{1}{2}\right)n_0\right] = 4n_a - 4\left(2^{m-2} - \frac{1}{2}\right)n_0 \tag{S21b}$$

The requirement is for the additional crosslink density to reach step m is

$$\frac{2^{m-1}-1}{2} < n_a/n_0 \leq \frac{2^m-1}{2} \tag{S22}$$

After strengthening, the strain energy function can be formulated as [4-10]

$$W_s = \sum_{j=m-1}^{m}\left[C_j k_B T\left(\frac{N_0}{2^j}\right)\left(\frac{\beta_j}{tanh\beta_j} + ln\frac{\beta_j}{sinh\beta_j}\right)\right] \tag{S23}$$

$$\beta_j = L^{-1}\left(\frac{\Lambda_j}{\sqrt{N_0/2^j}}\right) \tag{S24}$$

where the chain stretch Λ_j is given in Eq. S14 and C_j for $j = m-1$ and $j = m$ are given in Eq. S21. Under uniaxial tension with $\lambda_1 = \lambda$ and $\lambda_2 = \lambda_3 = \lambda^{-1/2}$, the nominal tensile stress of the incompressible polymer after strengthening can be calculated as

$$s_{s1} = \sum_{j=m-1}^{m}\left[C_j k_B T\sqrt{N_0/2^j}\,\frac{\lambda-\lambda^{-2}}{\sqrt{\lambda^2+2\lambda^{-1}}}L^{-1}\left(\sqrt{\frac{\lambda^2+2\lambda^{-1}}{N_0/2^j}}\right)\right] \tag{S25}$$

(3) Theoretical results

Strengthening with m=1

When $n_a/n_0 \leq 1/2$, there is only one-step strengthening. After the strengthening, only chains with lengths of N_0 and $N_0/2$ coexist in the system. The strengthening can be modeled by either method 1 or method 2. As shown in **Figs. S18AB**, the polymer with an initial chain length $N_0 = 100$ becomes stronger after forming more additional crosslinks. The Young's modulus (within 10% strain region) increases linearly with increasing the crosslink density (**Fig. S18B**).

We define the strengthening factor as the strengthened Young's modulus normalized by the unstrengthened Young's modulus. We find that the strengthening factor decreases with increasing the initial chain length N_0 (**Figs. S18CD**). When the initial chain length N_0 is very small, the polymer can be significantly strengthened. According to the stress-strain curve shapes of the studied polymers in this work (**Figs. S16**), the initial chain length should be $N_0 \geq 60$. The initial chain length cannot be too small. When the initial chain length $N_0 > 500$, the strengthening factor reaches a plateau of around 1.96. When the initial chain length $60 \leq N_0 \leq 2000$, the strengthening factor varies from 1.96 to 2.2.

According to the results shown in **Figs. 2G-J and S16**, the strengthening factor of the studied polymer in this work can reach as high as 6.2; therefore, we have to study the cases for $m > 1$.

Strengthening with m>1

When the density of the formed additional crosslinks $n_a/n_0 > 1/2$, the chain length distributions modeled by methods 1 and 2 are different. **Figure S19** shows the relationships between step number m and the density of the formed additional crosslinks for methods 1 and 2. For method 1, when n_a/n_0 increases to 5, the step number m drastically increases to 45. However, the step number m is still 4 when $n_a/n_0 = 5$ for method 2.

When n_a/n_0 is slightly larger than $1/2$ (e.g., 2/3), the strengthening factors calculated from methods 1 and 2 are still almost the same (**Fig. S20**). However, when n_a/n_0 increases to 1, the strengthening factors calculated from methods 1 are larger than those calculated from method 2 (**Figs. S21A-D**). It is because that the step number of method 1 is larger, corresponding to shorter chains.

When n_a/n_0 is relatively large (e.g., 3.05), the step number for method 1 is 21, which means that the shortest chain length becomes $N_0/2^{21}$. Considering the stress-strain curve shape of studied polymer (**Figs. S16**), the initial chain length N_0 is estimated between 60 and 2000. $N_0/2^{21}$ becomes an invalid number for the chain length. Therefore, under such a situation that additional crosslink density is relatively large, method 1 cannot model the strengthening behavior. We can only employ method 2 (**Figs. S21EF**).

(4) Comparison between theory and experiment

Using method 2, we can explain the stress-strain curves and Young's moduli of the polymers before and after strengthening (used parameters shown in **Table S2**). For example, for polymers with chloroplasts of various weight concentrations (0 to 5 wt%), the theoretically calculated stress-strain curves and Young's moduli agree with the respective experimental results (**Fig. S22AB**). It also works for polymers with 5 wt% chloroplasts under various illumination periods from 0 to 2 h (**Fig. S22CD**).

Supplies of water and carbon dioxide

Since the chloroplasts are embedded in the polyurethane-based polymer matrix, external water supply cannot be provided to support the photosynthesis of the chloroplasts. The water for the photosynthesis process should be supplied by the water storage within the chloroplasts [11-14]. To estimate the mass percentage of water within the extracted chloroplast, we placed the extracted chloroplast in a dark environment and applied a gentle airflow to evaporate the water for 8 h. Through measuring the mass before and after the evaporation process, we estimated the mass percentage of the water within the extracted chloroplast was 83.9±2.5 wt% (**Table S1**). If the weight percentage of the chloroplast is 5 wt%, with the density of polyurethane-based polymer as 1.25 g/cm^3, we can roughly estimate the volume density of water supply as

$$C_{H_2O}^0 = \frac{5\%\times 83.9\%\times 1.25\ g/cm^3}{18\ g/mol} = 2.91 mol/L \quad \text{(S26)}$$

In plants, the carbon dioxide is digested by stomas and then gradually diffuse into cells at a deeper location [12-14]. In this study, since the polyurethane-based polymer has a relatively high permeability for carbon dioxide, with the diffusivity experimentally measured as $D = 3.5\times 10^{-7} - 3.9\times 10^{-7} cm^2 s^{-1}$ [15,16], we hypothesize that the carbon dioxide that supports photosynthesis may be provided by the existing carbon dioxide within the polymer matrix and the diffusion of carbon dioxide through the polymer matrix during the photosynthesis process. The concentration of carbon dioxide in the atmosphere in year 2019 was around 410-415 ppm [17], which calculated as

$$C_{CO_2}^0 = 9.318\times 10^{-3} - 9.432\times 10^{-3} mol/L \quad \text{(S27)}$$

At the as-fabricated state, we assume the carbon dioxide within the polymer matrix is already in equilibrium with that in the atmosphere. During the photosynthesis process, the carbon dioxide within the polymer matrix is gradually consumed, and external carbon dioxide diffuses from the atmosphere into the polymer matrix.

The key question is whether the supplies of water and carbon dioxide are sufficient for the conducted experiment. To answer this question, we carry out the following estimation.

According to the theoretical modeling shown in above section, the initial chain density is estimated as $n_0 = 4.5\times 10^{19}\ m^{-3} = 7.475\times 10^{-8}\ mol/L$ (**Table S2**). The concentration of the required additional crosslinks n_a for strengthening the polymer network with 5 wt% embedded chloroplasts should scale with n_0, written as

$$n_a = \beta n_0 \quad \text{(S28)}$$

where β is a parameter (<10) dependent on the light illumination time. For example, for 2-h light illumination, $\beta = 2.3$; and for 4-h light illumination, $\beta = 3 - 3.5$.

One glucose molecule with 5 OH groups is only required to bridge two NCO groups to form a crosslink. Thus, one glucose molecule is able to at most form 2.5 crosslinks within the network. The number of the introduced glucose molecules per unit volume is denoted as n_g, which follows $n_g \le n_a \le 2.5 n_g$. Therefore, the possible highest concentration of the required glucose is

$$n_g = n_a = \beta n_0 \quad \text{(S29)}$$

For a photosynthesis process, the overall effective chemical reaction can be written as [12-14]

$$6\,H_2O + 6\,CO_2 \xrightarrow{h\nu} C_6H_{12}O_6 + 6\,O_2 \tag{S30}$$

Equation S30 shows that the production of 1 glucose molecule requires 6 water molecules and 6 carbon dioxide molecules. Therefore, the concentrations of the required water and carbon dioxide are estimated as

$$C^r_{H_2O} = C^r_{CO_2} = 6\beta n_0 \tag{S31}$$

For 4-h light illumination (along with the subsequent 4-h darkness), $6\beta n_0 \sim 1.35 \times 10^{-6} - 1.57 \times 10^{-6}\ mol/L$. Then, we have

$$C^r_{H_2O} \ll C^0_{H_2O} \tag{S32}$$

$$C^r_{CO_2} < C^0_{CO_2} \tag{S33}$$

Therefore, the supplies of water and carbon dioxide are sufficient for the experiment with 4-h light illumination (and 4-h darkness) in this work.

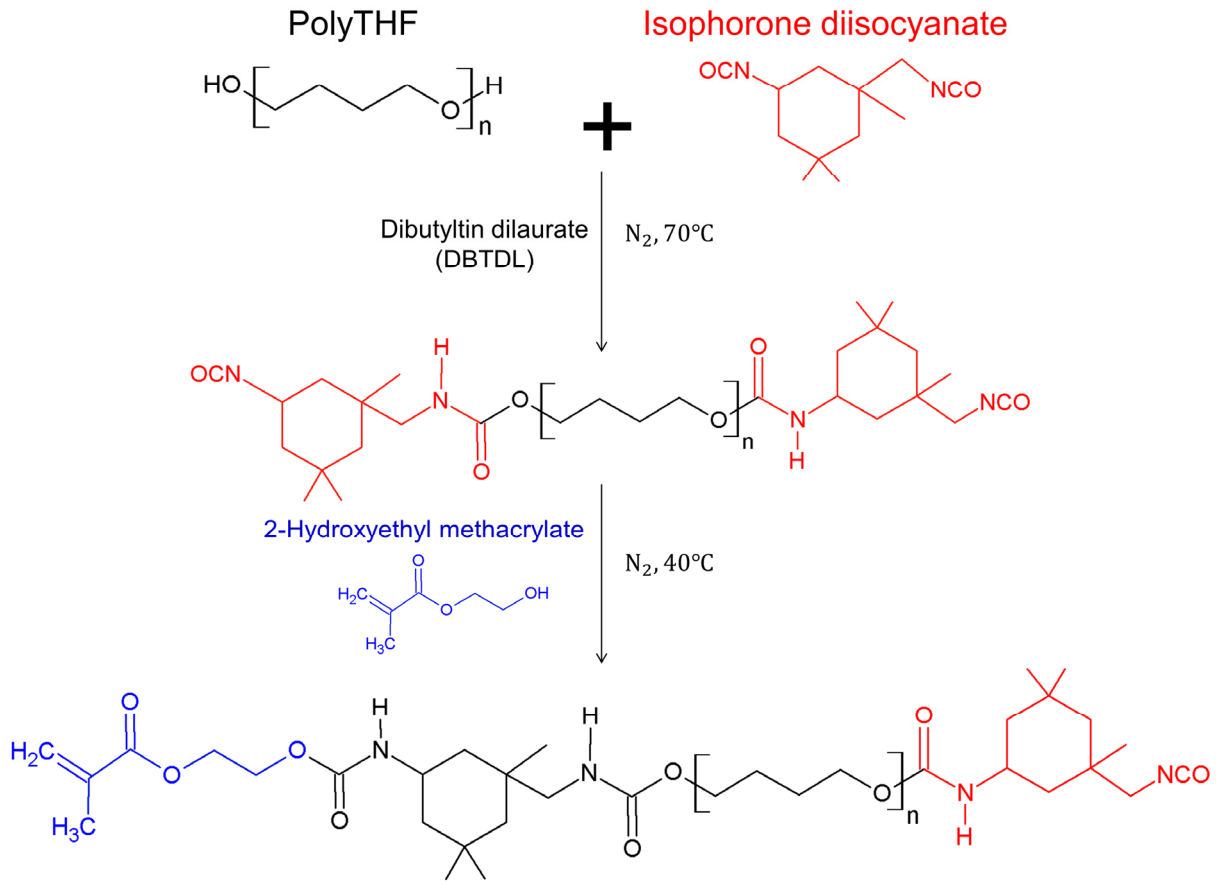

Figure S1. **Synthesis of polymer resin with acrylate and isocyanate (NCO) groups.** 0.01 mole of PolyTHF was preheated at 100℃ and exposed to a nitrogen environment for 1 h to remove moisture and oxygen. 0.02 mole of IPDI, 10 wt% of DMAc and 1 wt% of DBTDL were mixed with preheated PolyTHF at 70℃ and stirred with a magnetic stir bar for 1 h. After reducing the temperature to 40℃, 0.01 mole of HEMA was added and mixed for 1 h to complete the synthesis.

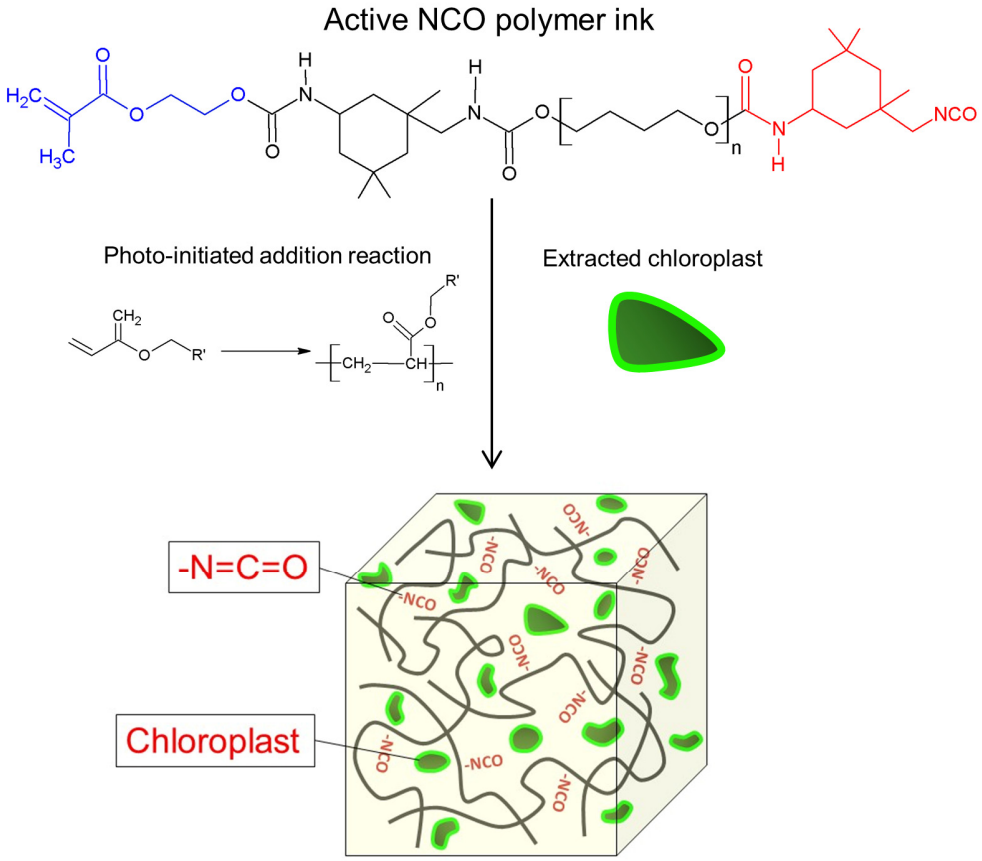

Figure S2. **Preparation of experiment polymer sample.** Extracted spinach chloroplasts were gently mixed with prepared polymer resin with acrylate and NCO groups by using a magnetic stir bar for 30 min at 5℃ in a dark environment to prevent the degradation of chloroplasts. The mixed polymer resin then went through a photoradical-initiated addition reaction with the photopolymerization-based stereolithography system to photopolymerize the polymer resin.

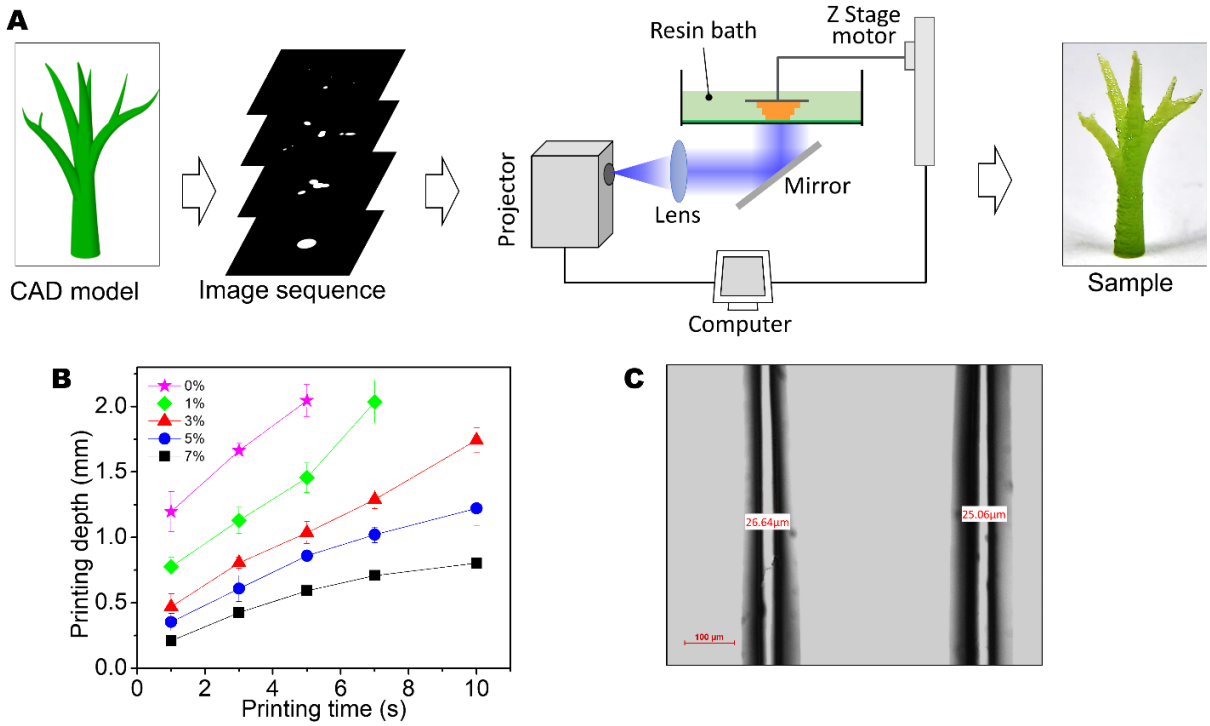

Figure S3. (A) 3D-printing of polymer structures. A CAD model was first sliced into a sequence of images. These 2D slice images, illuminated with UV/blue light from a light-emitting diode, were sequentially projected onto a transparent window. On the window, the liquid photoresin, capped into a prescribed height by a printing stage, was cured by the light and attached to the printing stage. As the printing stage was lifted off, the fresh resin refluxed beneath the printing stage. By lowering down the stage by a prescribed height and illuminating the resin with a subsequent slice image, a new layer could be printed and bonded onto the former layer. To eliminate the adhesion between the solidified resin and bath, we attached an oxygen-permeable membrane to the bottom, inducing a thin layer (~5-20μm) of the oxygen-rich dead zone to quench the photopolymerization. After repeating these processes, a 3D-architected polymer structure could be printed. (**B**) The relationships between the printing depth and the printing time for polymer inks with embedded chloroplasts of various weight concentrations. (**C**) Printed strips to illustrate the printing resolution (~25 μm).

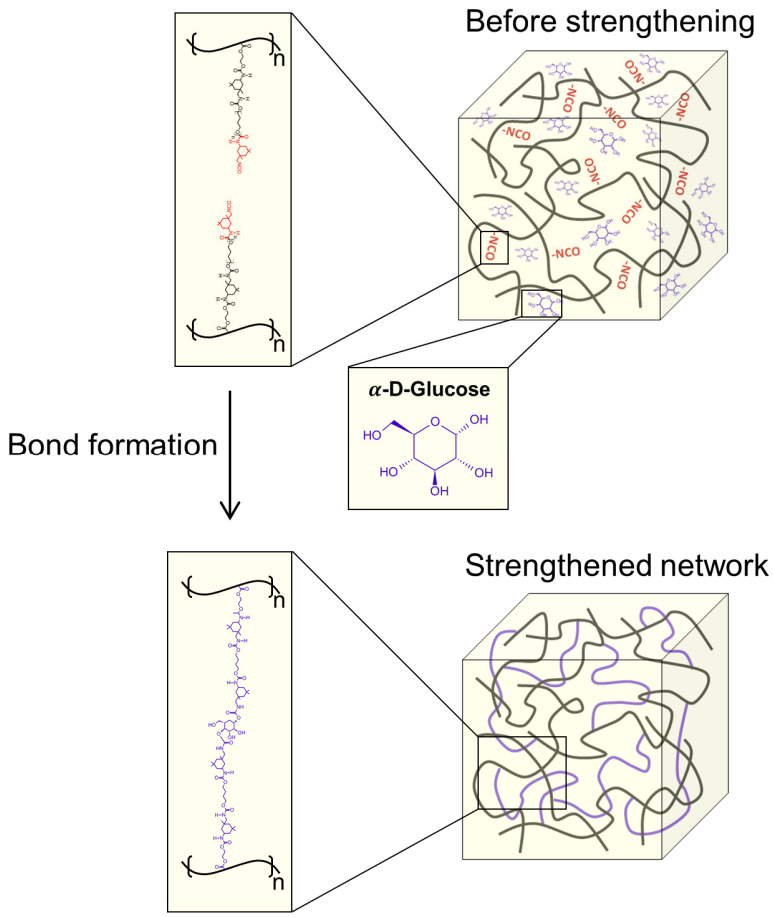

Figure S4. Schematics to show the bond formation process between OH groups on the chloroplast-produced glucose with free NCO groups. The zoom-in view of the initial network shows the chemical structure of free NCO groups and chloroplast-created glucose. The zoom-in view of the strengthened network shows the chemical structure with the new crosslink.

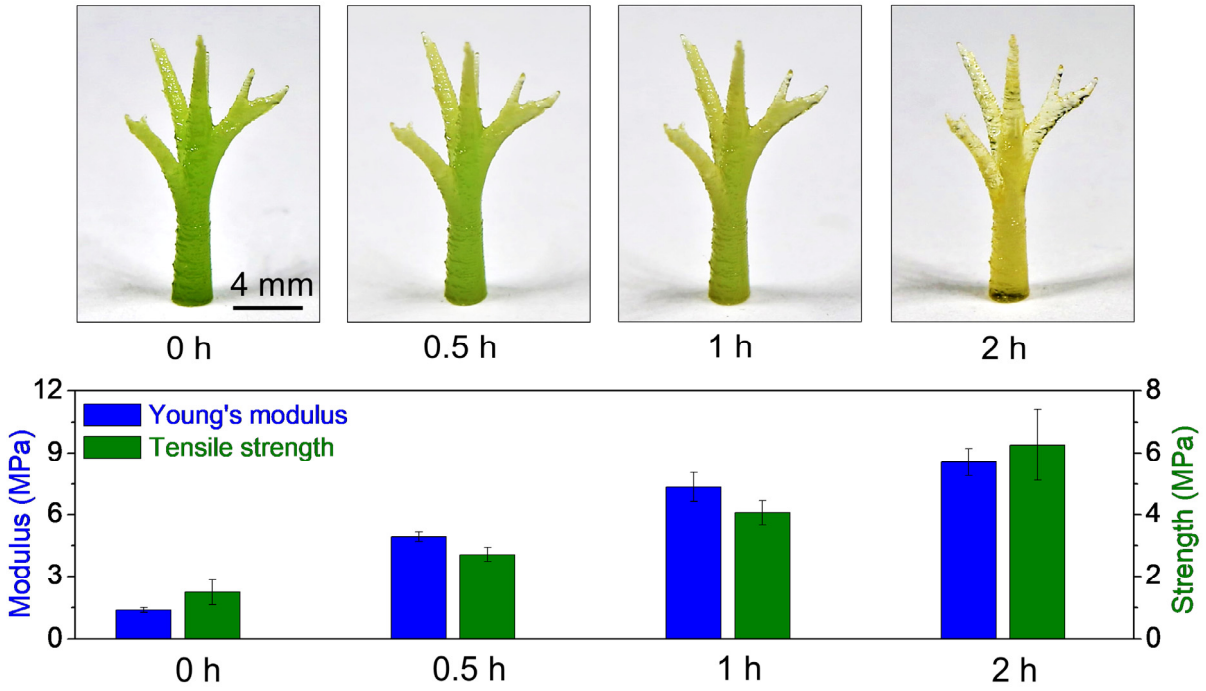

Figure S5. Young's moduli and tensile strengths of the polymers in the 3D-printed tree-like structures with various light illumination periods. The data of Young's modulus and tensile strengths were measured using dumbbell-shaped samples.

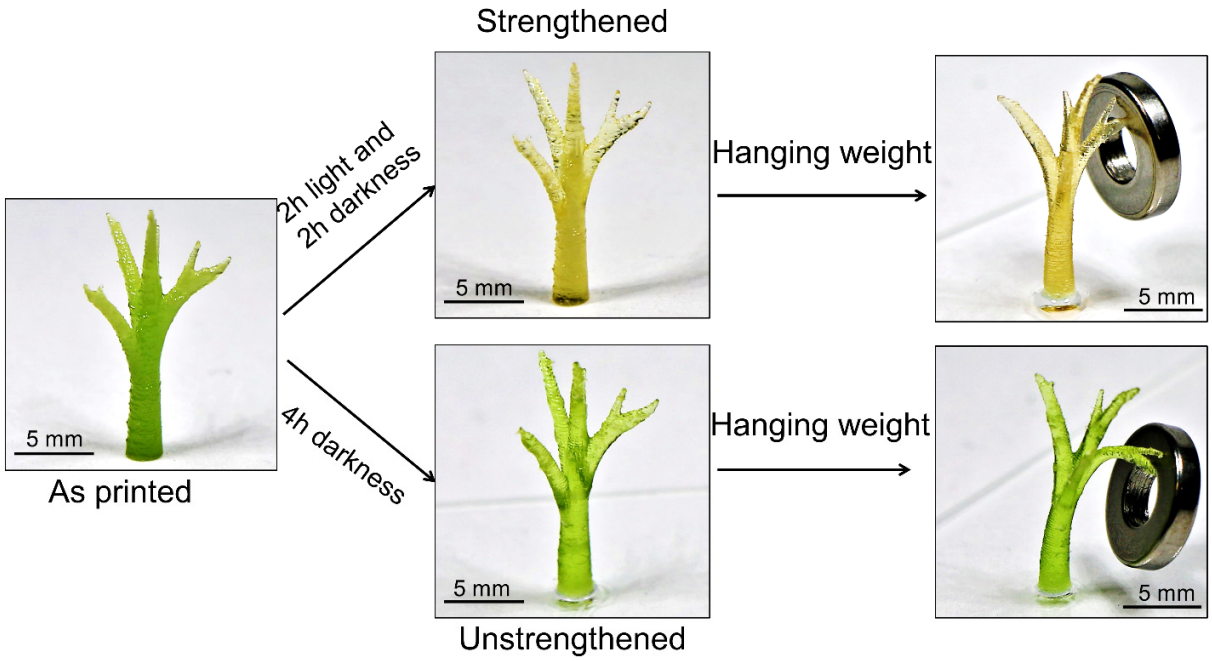

Figure S6. **Load sustaining ability 3D-printed tree-like structures.** In the top case, the tree structure went through 2-h light illumination (white light intensity 69.3 W/m^2) and 2-h darkness. In the bottom case, the tree structure went through 4-h darkness. The mass of the metal ring is 1 g.

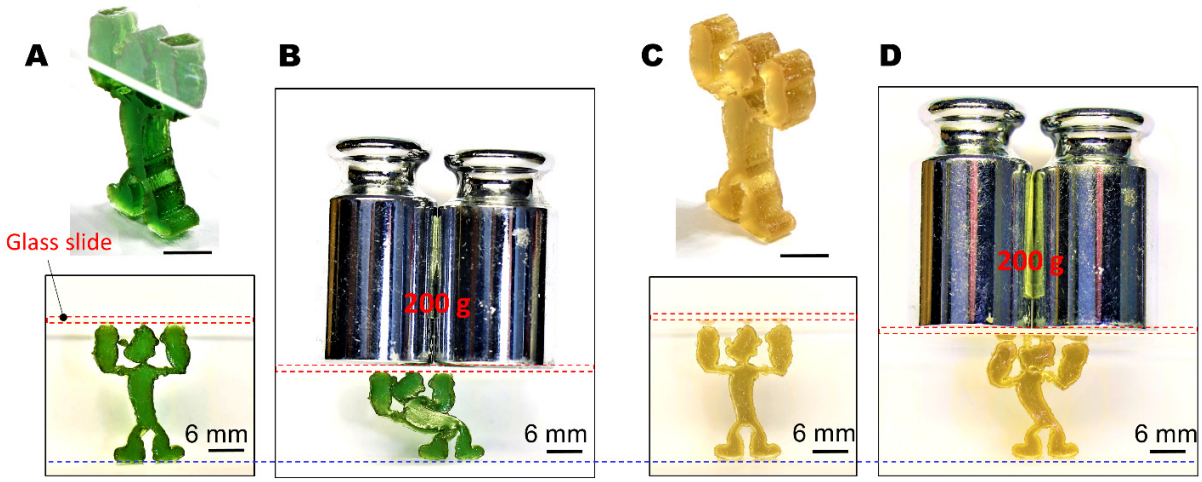

Figure S7. Load-sustaining ability of the 3D-printed Popeye-like structures. (A) Unstrengthened Popeye-like structure. (B) Unstrengthened Popeye-like structure loaded by a weight of 200 g. Its height reduces by 34.7%. (C) Strengthened Popeye-like structure. (D) Strengthened Popeye-like structure loaded by a weight of 200 g. Its height reduces by 7%.

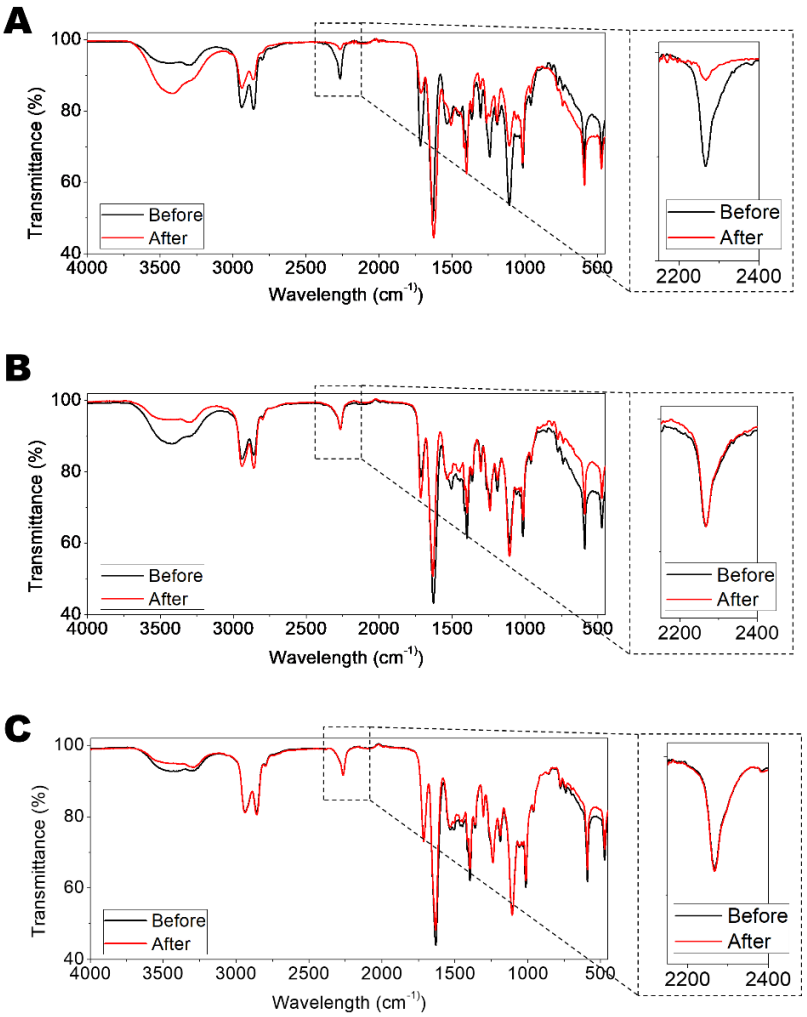

Figure S8. **Full FTIR spectra of samples with three groups.** (A) FTIR spectra of experimental group samples (with free NCO groups and embedded chloroplasts) before and after 4-h light illumination and 4-h darkness. (B) FTIR spectra of control 1 samples (with free NCO groups and embedded chloroplasts) before and after 8-h darkness. (C) FTIR spectra of control 2 samples (with free NCO groups but without embedded chloroplasts) before and after 4-h light illumination and 4-h darkness. The zoom-in view shows the spectra in the range of 2150 cm^{-1} to 2400 cm^{-1}, which indicates the concentration of the free NCO groups.

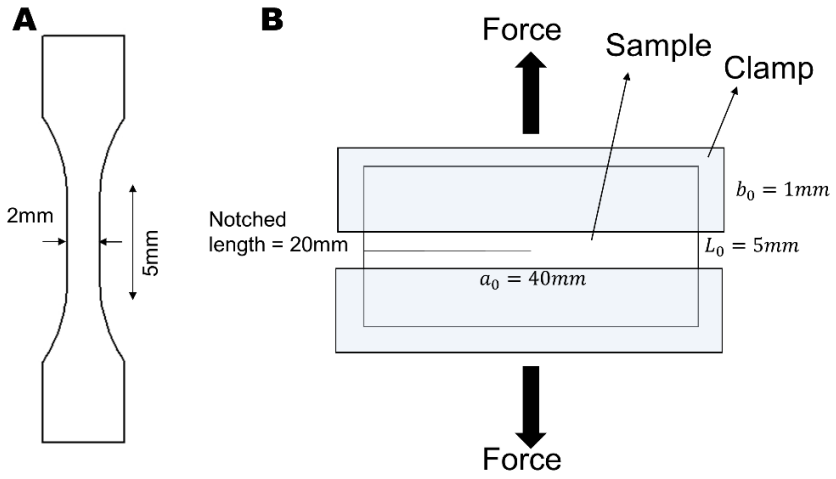

Figure S9. **Sample geometries of tensile and pure-shear fracture toughness tests.** (A) Geometry of a tensile test sample. The sample thickness is 2mm. (B) Geometry of a notched sample for pure-shear fracture toughness test. The fracture toughness test was conducted by testing an unnotched and notched sample. Each sample has a testing length a_0 =40 mm, thickness b_0 =1 mm and distance between two clamps L_0 =5mm. A 20-mm notch on the notched sample was prepared by using a razor blade. Both samples were tensile stretched with a strain rate of 0.05 s^{-1} and recording using a high-speed camera to record the critical distance between the clamps when the crack starts propagating on the notched sample L_c. The fracture energy of the material was calculated as $U(L_c)/(a_0 b_0)$, where $U(L_c)$ is the work done by the applied force before critical distance, illustrated as the area beneath the force-distance curve in the unnotched test.

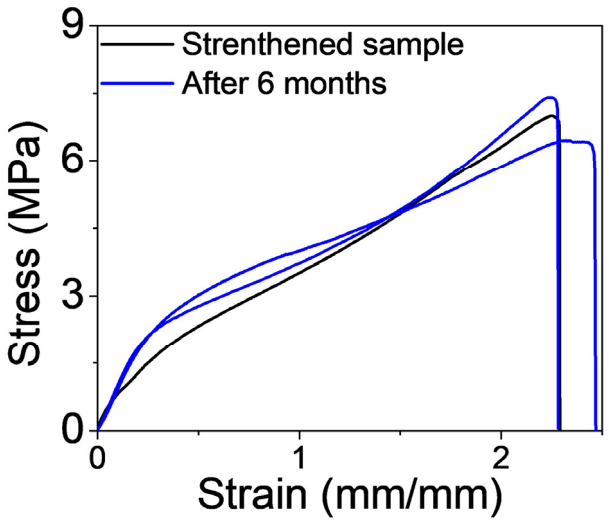

Figure S10. **Stress-strain curves of a polymer sample right after the strengthening with 4-h light illumination and 4-h darkness and the strengthened polymers after 6 months**. The employed polymer sample was 3D-printed with polymer inks with free NCO groups and embedded chloroplasts. The results show that the strengthened polymer maintains its Young's modulus and tensile strength after 6 months.

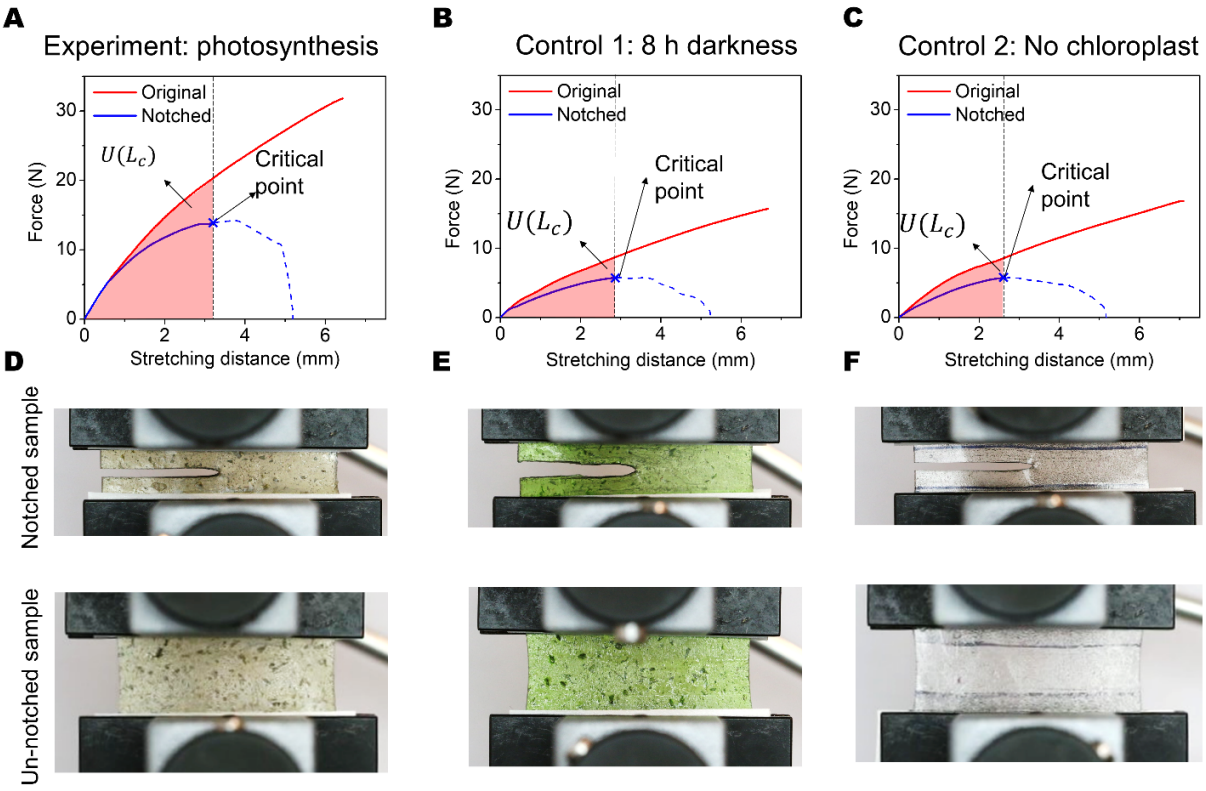

Figure S11. Force-distance curves and experiment images for fracture-toughness tests. Force-distance curves of notched and unnotched samples under uniaxial stretch for (A) the experimental case, (B) control 1 case, and (C) control 2 case. The experimental sample has free NCO groups and embedded chloroplasts, and undergoes 4-h light illumination and 4-h darkness. The control 1 sample has free NCO groups and embedded chloroplasts, and undergoes 8-h darkness. The control 2 sample has free NCO groups but no embedded chloroplasts, and undergoes 4-h light illumination and 4-h darkness. The critical points indicate the point when the crack starts propagating on the notched sample. Sample images of notched and unnotched samples under uniaxial stretch for (D) the experimental case, (E) control 1 case, and (F) control 2 case.

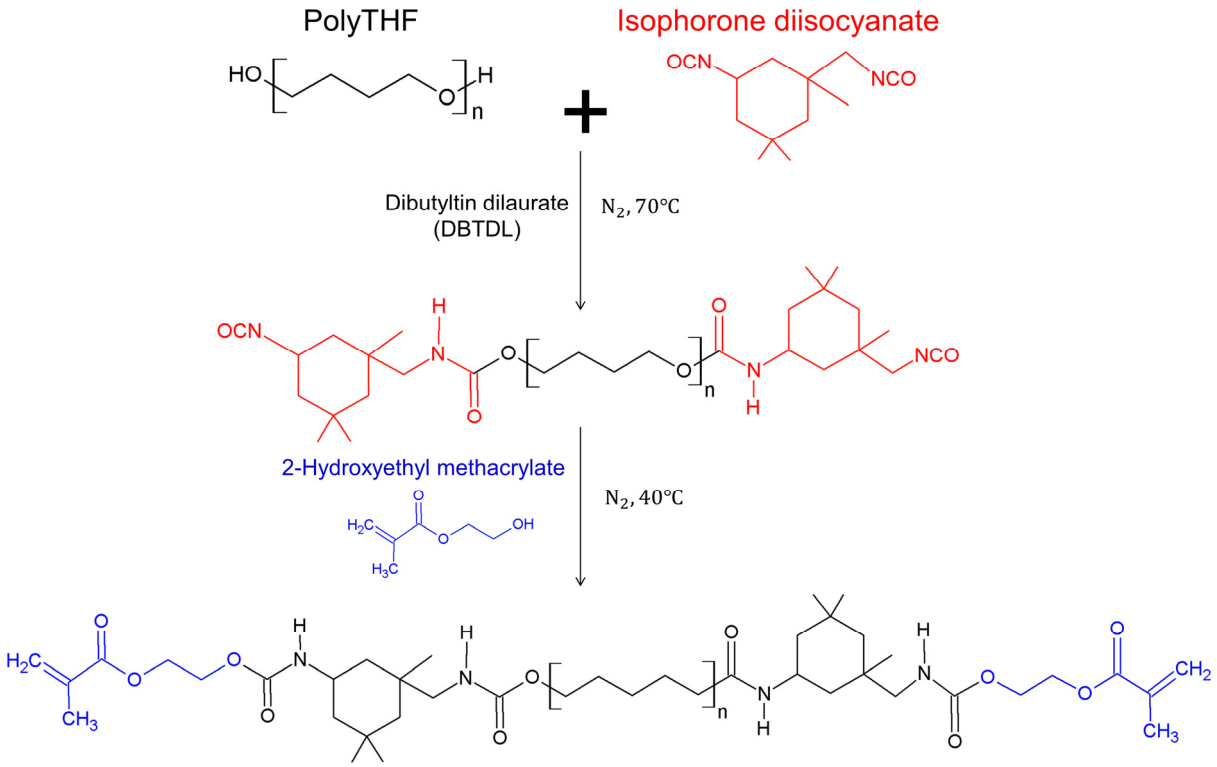

Figure S12. **Synthesis of polymer resin with only acrylate groups but without free NCO groups.** 0.01 mole of PolyTHF was preheated at 100℃ and exposed to a nitrogen environment for 1 h to remove moisture and oxygen. 0.02 mole of IPDI, 10 wt% of DMAc and 1 wt% of DBTDL were mixed with preheated PolyTHF at 70℃ and stirred with a magnetic stir bar for 1 h. After reducing the temperature to 40℃, 0.02 mole of HEMA was added and mixed for 1 h to complete the synthesis.

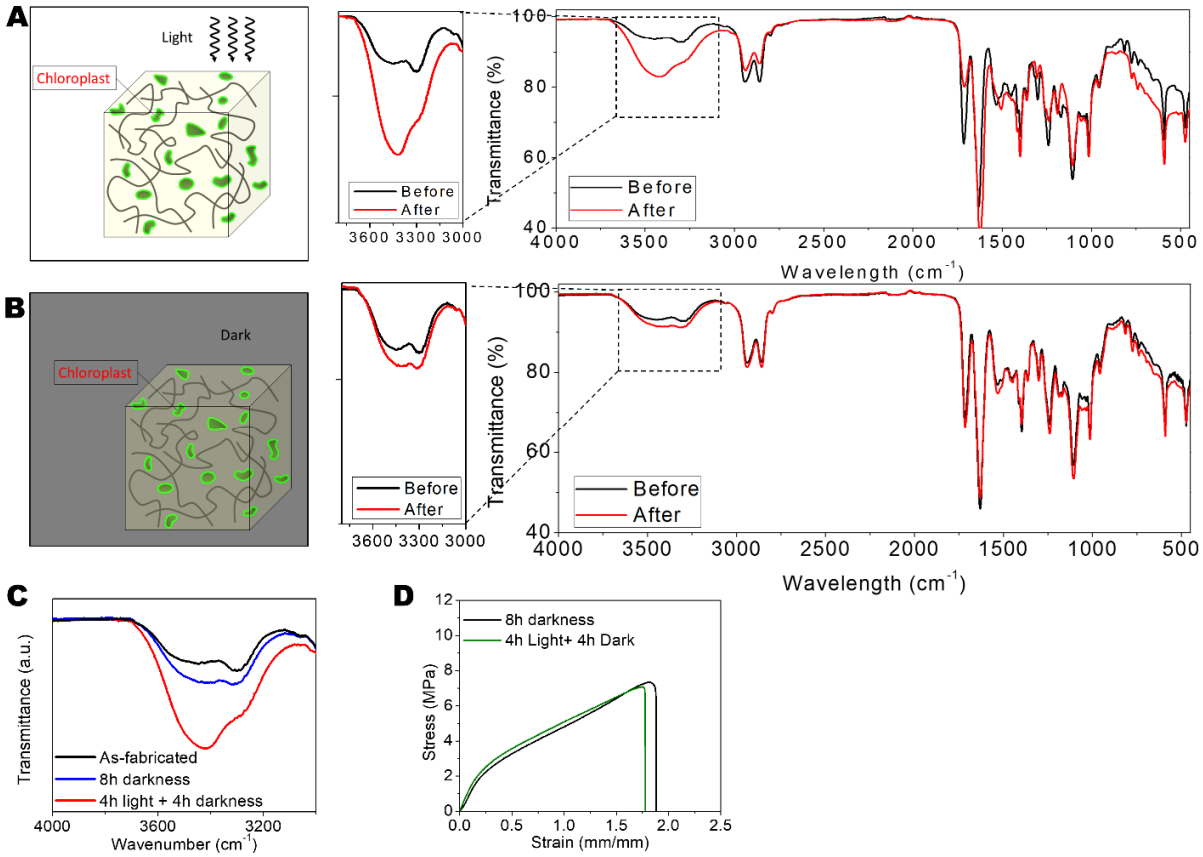

Figure S13. **Experiments on polymer samples with embedded chloroplasts but without free NCO groups.** (A) The polymer samples with embedded chloroplasts but without free NCO groups went through 4-h light illumination (white light intensity 69.3 W/m^2) and 4-h darkness. (B) The polymer samples with embedded chloroplasts but without free NCO groups went through 8-h darkness. (C) The zoom-in views showing the spectra in the range of 3000 cm^{-1} to 3800 cm^{-1}, which indicates the concentration of OH groups [18]. (D) Tensile stress-strain curves of polymer samples with embedded chloroplasts but without free NCO groups after 4-h light illumination and 4-h darkness, and 8-h darkness.

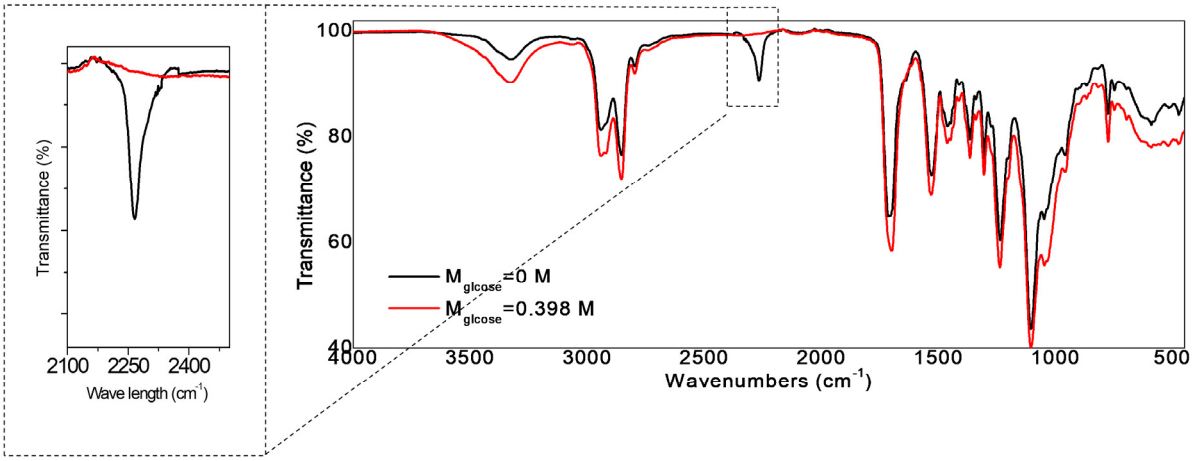

Figure S14. Full FTIR spectra of polymer ink with free NCO groups but without embedded chloroplasts before and after being mixed with 0.398 mol/L of glucose. The zoom-in view shows the spectrum in the range of 2100 cm^{-1} to 2500 cm^{-1}, which indicates the concentration of free NCO groups.

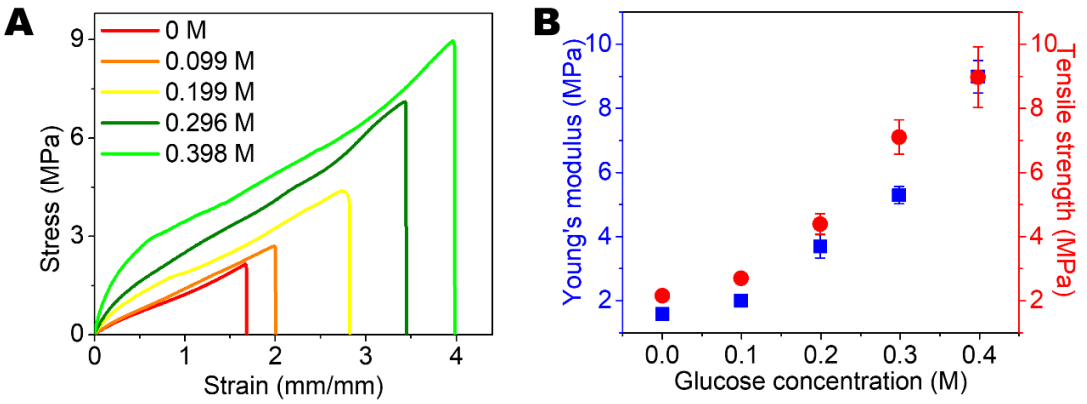

Figure S15. (A) Uniaxial tensile stress-strain curves of polymer samples with free NCO groups and various concentrations of glucose. (B) Young's moduli and tensile strengths in functions of the glucose concentration. The error bars represent the standard deviations of 3-5 samples.

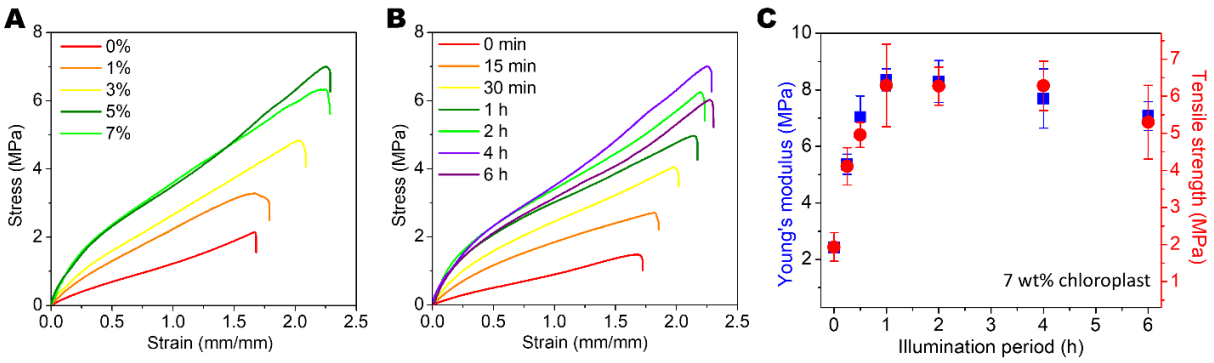

Figure S16. (**A**) Uniaxial tensile stress-strain curves of polymer samples with free NCO groups and embedded chloroplasts of various weight concentrations. (**B**) Uniaxial tensile stress-strain curves of polymer samples with free NCO groups and 5 wt% chloroplasts after the photosynthesis processes with various light illumination periods. (**C**) Young's moduli and tensile strengths of experimental samples with 7 wt% chloroplasts after the photosynthesis processes with various light illumination periods.

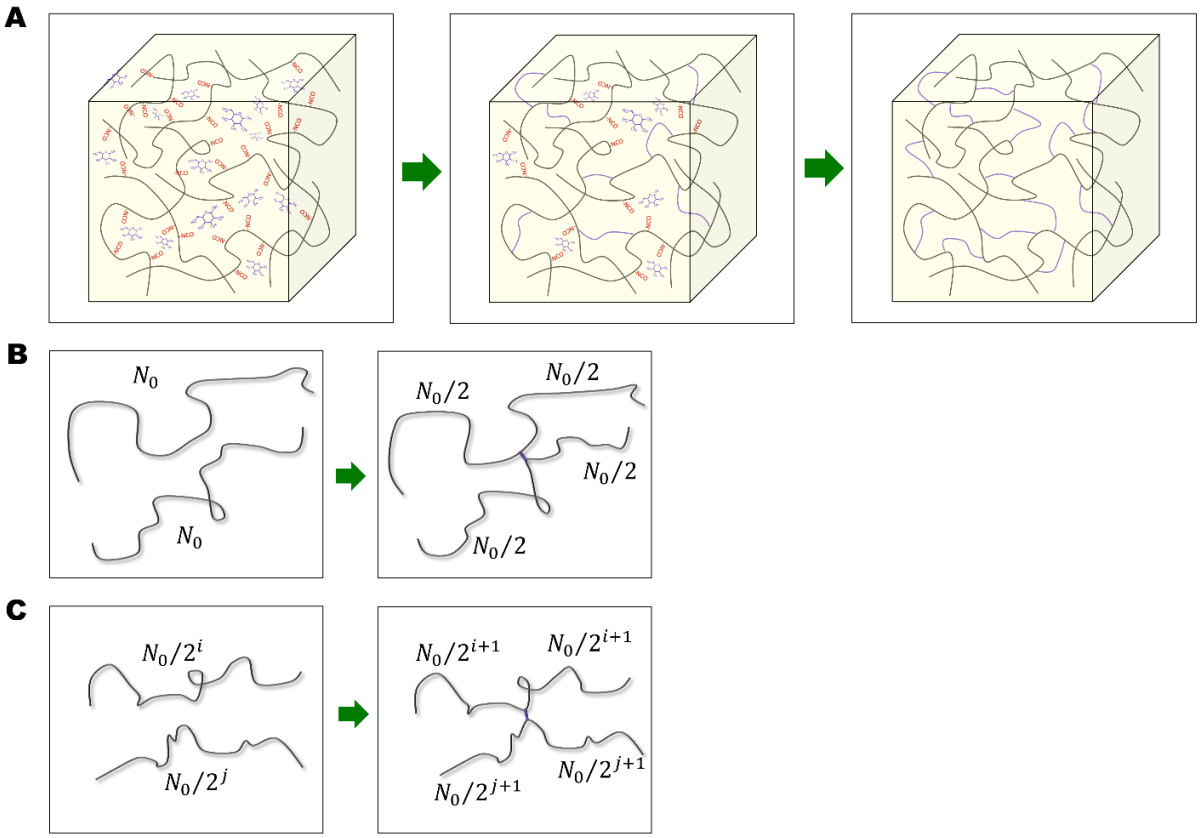

Figure S17. **Schematics for the polymer network.** (A) Schematics to show the formation of additional crosslinks through the reaction between the free NCO groups and the glucose. (B) Schematics to show the formation of one crosslink between two chains with the length of N_0. We assume each chain with the initial length of N_0 becomes two chains with the length of $N_0/2$. (C) Schematics to show the formation of one crosslink between a chain with the length of $N_0/2^i$ and a chain with the length of $N_0/2^j$. We assume the crosslink formed between a chain with the length of $N_0/2^i$ and a chain with the length of $N_0/2^j$ induces four chains with respective half lengths, where $i = 0,1,2\cdots$ and $j = 0,1,2\cdots$.

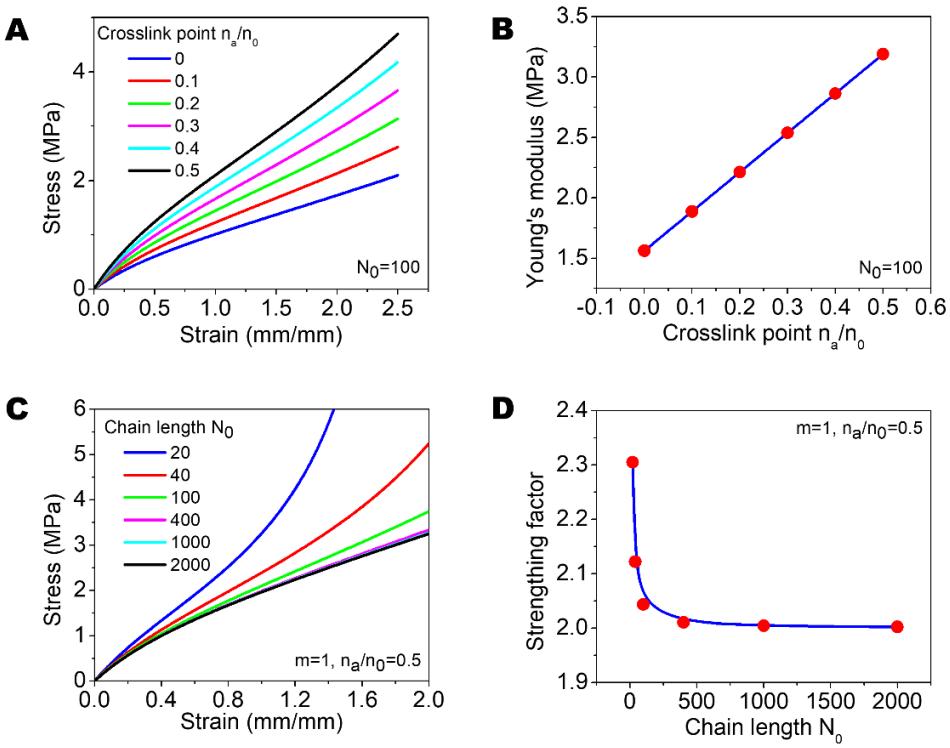

Figure S18. **Theoretical results for step number m=1**. (A) Nominal tensile stress-strain curves for various normalized additional crosslink density n_a/n_0. (B) The Young's modulus of the polymer in a function of the normalized additional crosslink density n_a/n_0. The Young's modulus is calculated from the stress-strain curve within 10% strain. (C) Nominal tensile stress-strain curves for various initial chain length N_0 and $n_a/n_0 = 0.5$. (D) Strengthening factor in a function of the chain length for $m = 1$ and $n_a/n_0 = 0.5$. The strengthening factor is defined as the strengthened Young's modulus normalized by the unstrengthened Young's modulus.

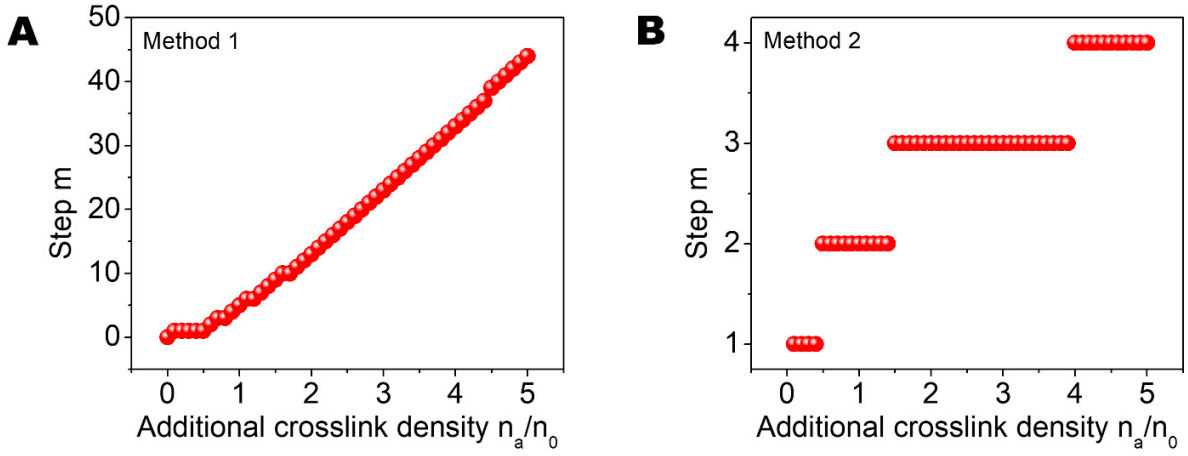

Figure S19. Relationships between the step number m and additional crosslink density n_a/n_0 for (A) method 1 and (B) method 2.

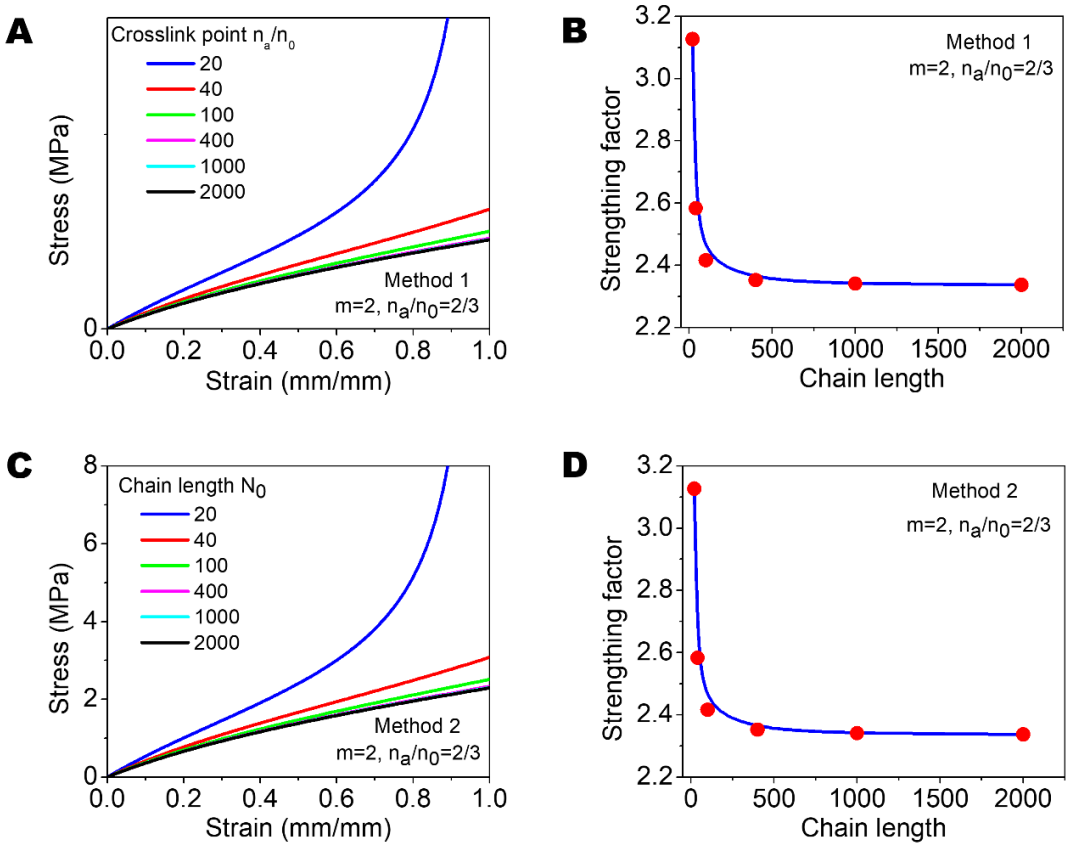

Figure S20. **Theoretical results for $m = 2$ and $n_a/n_0 = 2/3$**. Stress-strain curves and strengthening factors for various initial chain lengths N_0 based on (AB) method 1 and (CD) method 2.

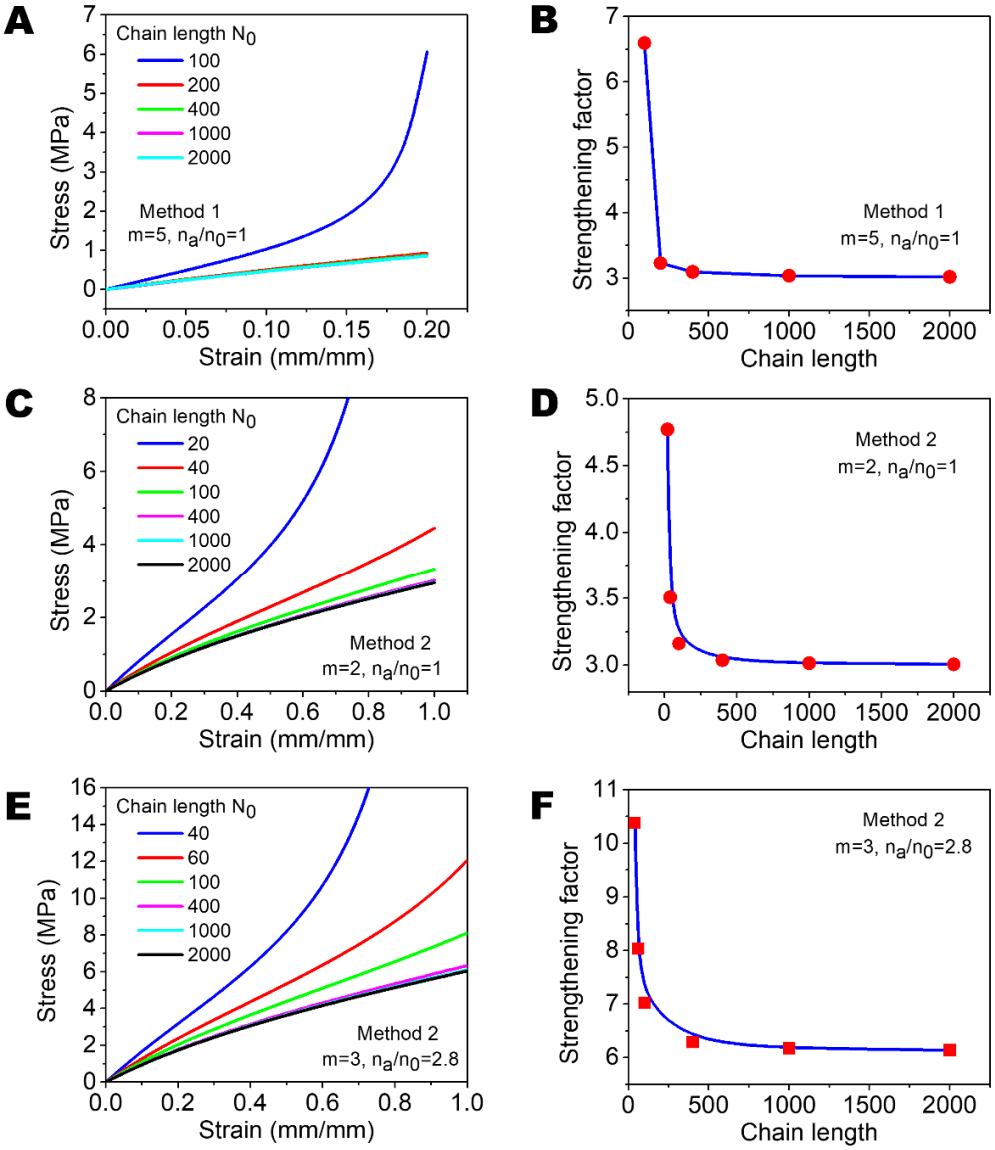

Figure S21. Theoretical results for $n_a/n_0 > 2/3$. Stress-strain curves and strengthening factors for various initial chain lengths N_0 and (AB) $m = 5$ and $n_a/n_0 = 1$ (method 1), (CD) $m = 2$ and $n_a/n_0 = 1$ (method 2), and (EF) $m = 3$ and $n_a/n_0 = 3.05$ (method 2).

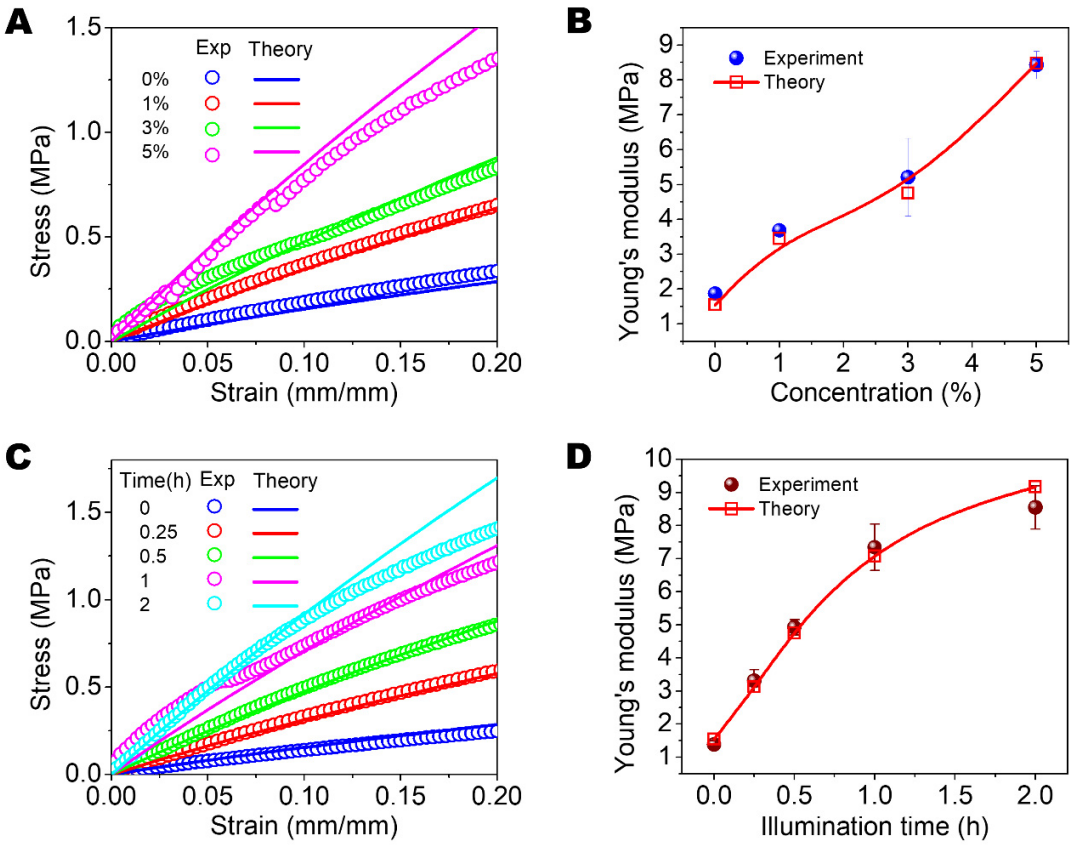

Figure S22. Comparison between the theory and experiment. (A) Stress-strain curves and (B)Young's moduli of polymer samples with free NCO groups and chloroplasts of various weight concentrations after 4-h light illumination and 4-h darkness. (C) Stress-strain curves and (D)Young's moduli of polymer samples with free NCO groups and 5 wt% chloroplasts after various illumination periods and the corresponding periods of darkness. The parameters used to calculate the theoretical results are listed in **Table S2**. The error bars in (B) and (D) represent standard deviations of 3-5 samples.

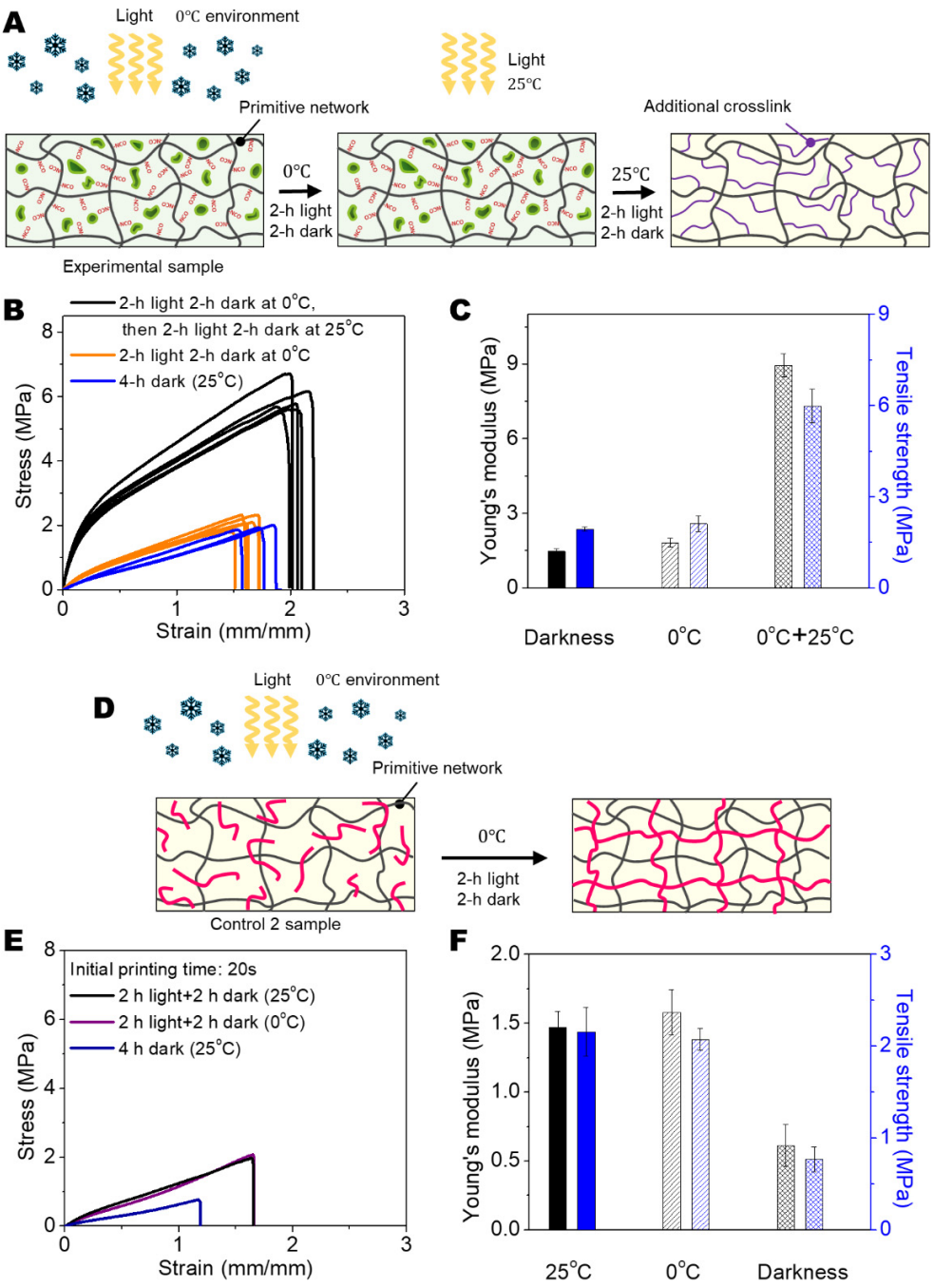

Figure S23. Effect of chilling temperature on the proposed hybrid synthetic-living material and traditional photopolymer. (A) Schematics to illustrate the procedure for an experimental sample first undergoing 2-h light illumination and 2-h darkness at 0°C, and then undergoing 2-h light illumination and 2-h darkness at 25°C. (BC) Stress-strain curves, Young's moduli, and tensile strengths of the processed experimental samples at three states: after 4-h darkness, after 2-h light and 2-h darkness at 0°C, and after 2-h light and 2-h darkness at 0°C followed by 2-h light and 2-h darkness at 25°C. The error bars represent standard deviations of 3-5 samples. Results show that chilling temperature can temporarily freeze the living activity of the embedded chloroplasts. (D)

Schematics to illustrate the post-curing procedure for a partially-crosslinked control 2 sample undergoing 2-h light illumination and 2-h darkness at 0℃. Since the control 2 sample can be fully crosslinked with light illumination of 60s, we employed 20s to enable a partial crosslinking. (EF) Stress-strain curves, Young's moduli, and tensile strengths of the processed control 2 samples at three states: after 2-h light and 2-h darkness at 25℃, after 2-h light and 2-h darkness at 0℃, and after 4-h darkness at 25℃. The error bars represent standard deviations of 3-5 samples. Results show that the post-curing of a partially-crosslinked photoresin cannot be frozen by a chilling temperature.

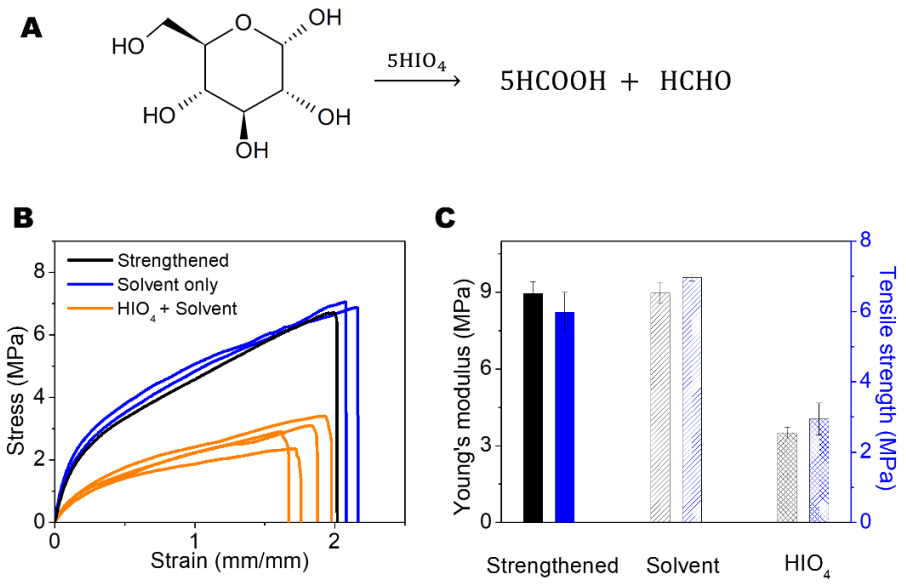

Figure S24. **Cleavage of glucose crosslinkers with period acids (HIO_4)**. (A) Chemical reaction for cleaving a glucose molecule with period acids. (BC) Stress-strain curves, Young's moduli, and tensile strengths of strengthened samples, and strengthened samples treated with solvent DMAc only, and strengthened samples treated with HIO_4 solution (2 M HIO_4 with solvent DMAc). The mechanical tests were carried out after evaporating the residual solvents. Results show that the HIO_4 can cleave the glucose crosslinkers to reverse the strengthened samples back to the soft state. The error bars represent standard deviations of 3-5 samples.

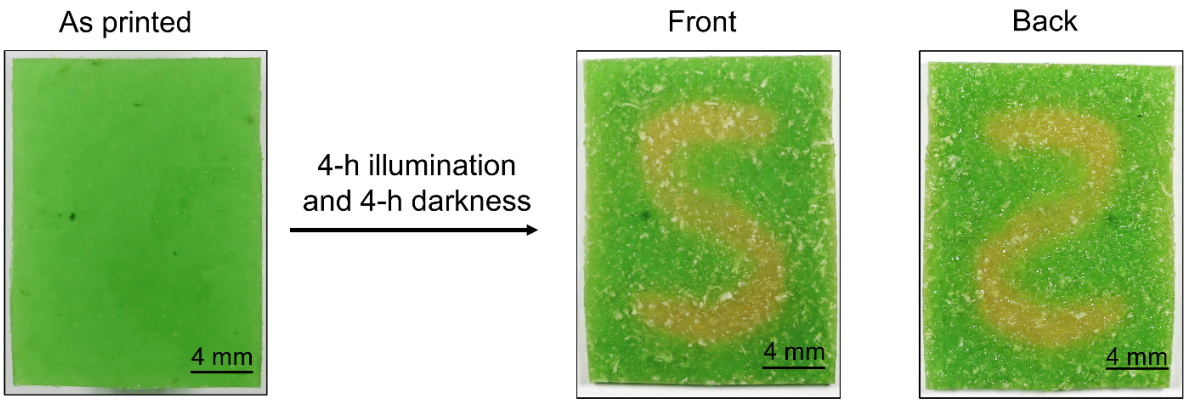

Figure S25. Sample images of a locally strengthened sample through a patterned light with an "S" shape.

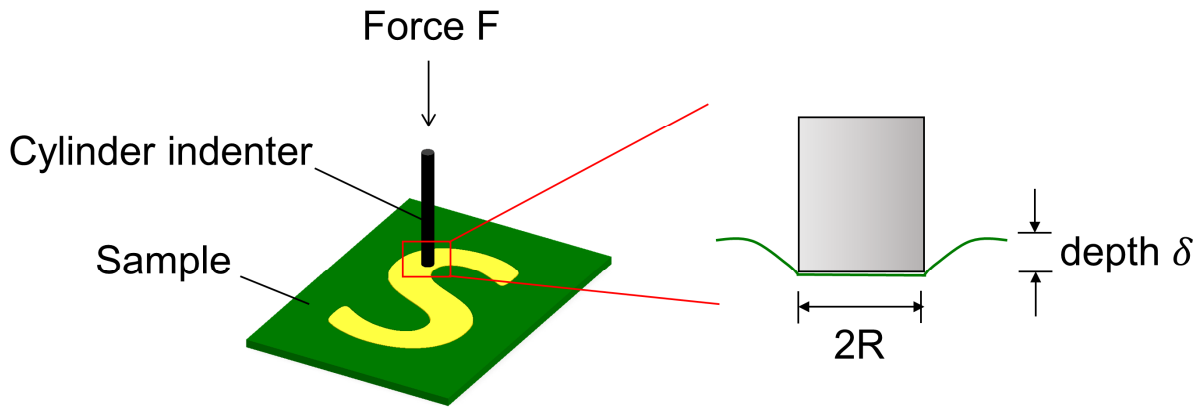

Figure S26. **Experimental set-up of an indentation test.** A round-flat end cylinder indenter with radius R=1 mm is loaded on the Instron mechanical tester to indent the sample by applying force F to a certain indentation depth δ. The Young's modulus is calculated as $E = F(1-\upsilon^2)/(2R\delta)$, where υ is the Poisson's ratio.

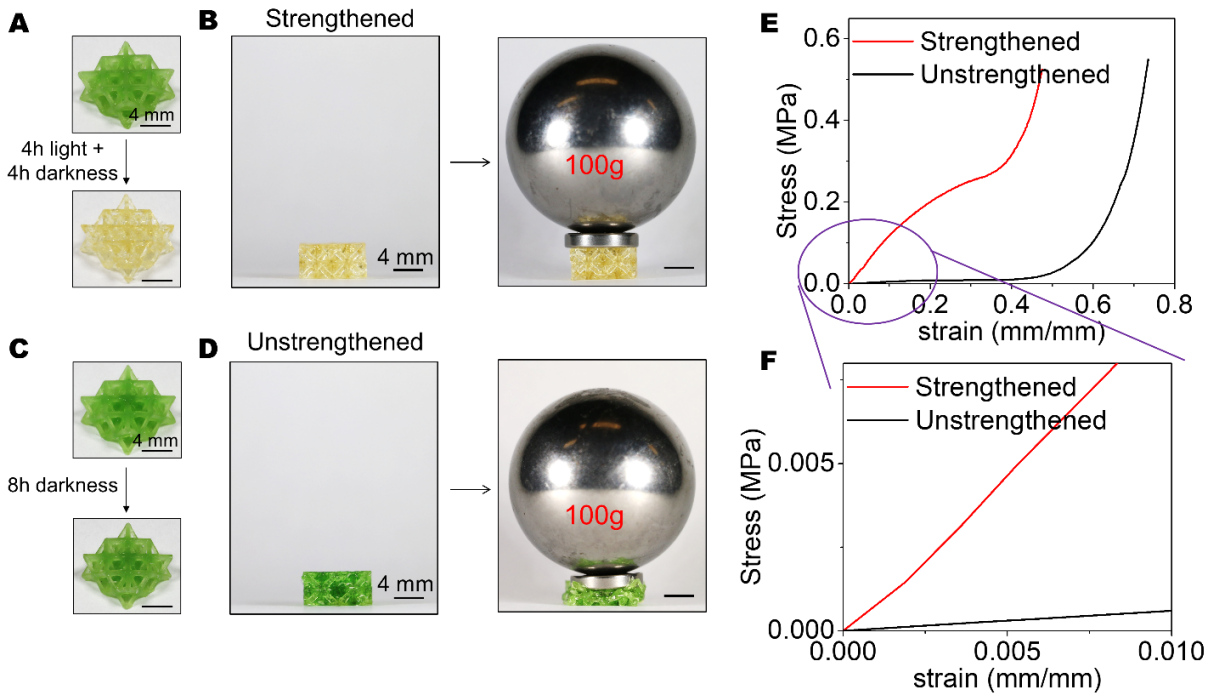

Figure S27. Strengthening of Octet lattice with homogeneous light illumination. (AB) 3D-printed Octet lattice structure with free NCO groups and embedded chloroplasts went through 4-h light illumination and 4-h darkness and sustained a 100g weight (lattice weight 0.12 g). (CD) 3D-printed Octet lattice structure with free NCO groups and embedded chloroplasts went through 8-h darkness and sustained a 100g weight. (E) Compressive stress-strain curves of the strengthened and unstrengthened Octet lattice structures. (F) Zoom-in view of the compressive stress-strain curve of the 3D-printed Octet lattice structure. The strengthened lattice exhibits Young's modulus that is 20 times that of the non-strengthened lattice. The scale bars represent 4 mm.

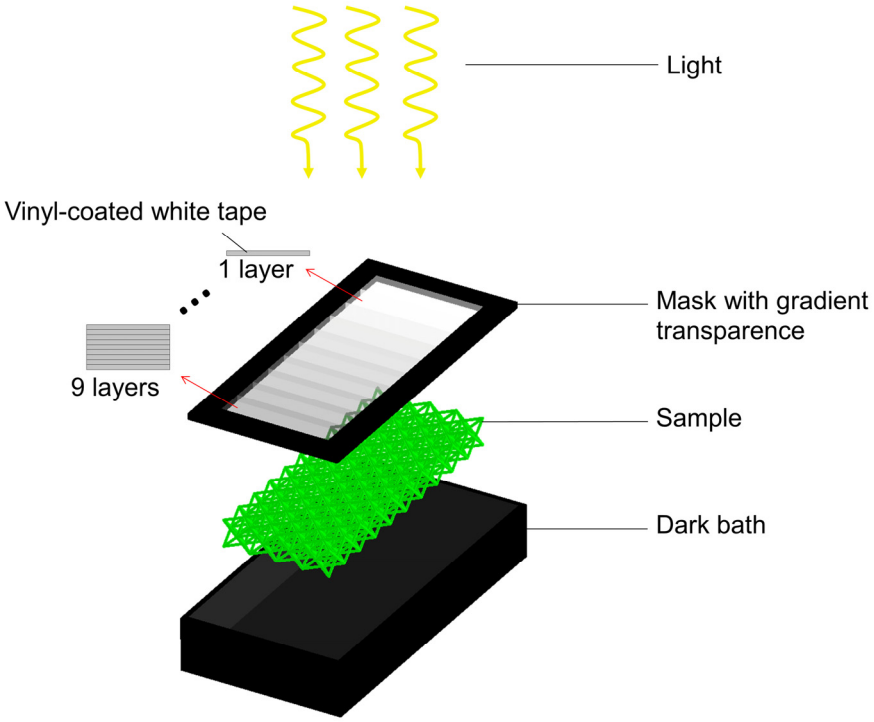

Figure S28. **Schematic to show the experimental setup for the 3D-printed structures with a gradient light intensity.** A transparent cover was attached with different layers of vinyl-coated white tape and covered on top of the printed sample. The entire setup was then placed in the chamber with light intensity varies from 0 to 69.3 W/m^2 on the long edge direction of the sample for each unit distance (2 mm).

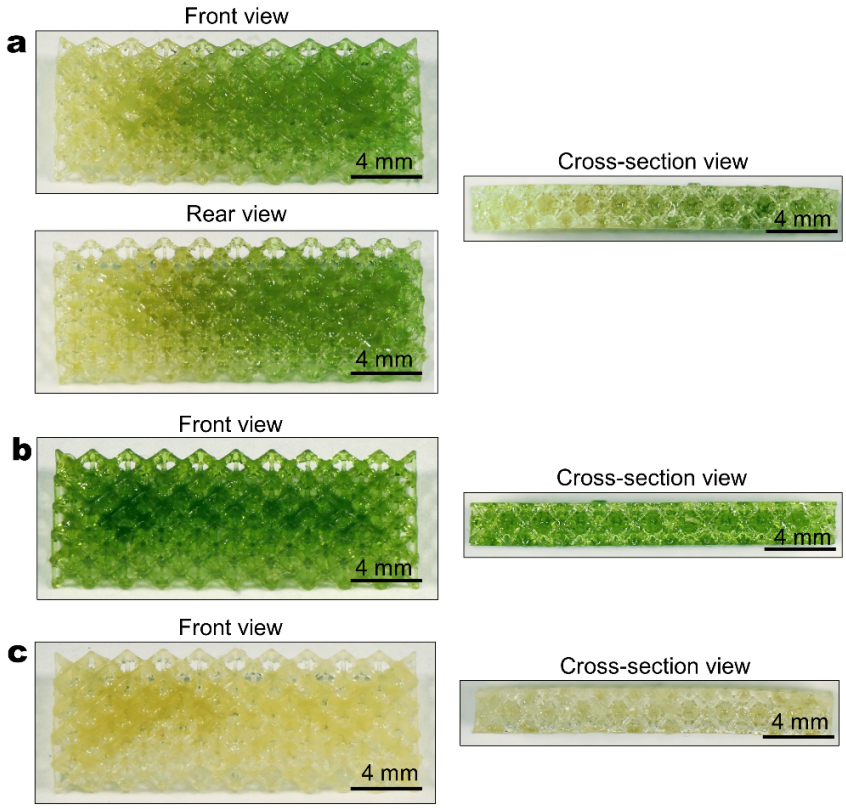

Figure S29. (a) Front, rear, and cross-section views of the functionally-graded lattice structure. (bc) Front and cross-section views of the (b) fully-soft and (c) fully-stiffened lattice structures.

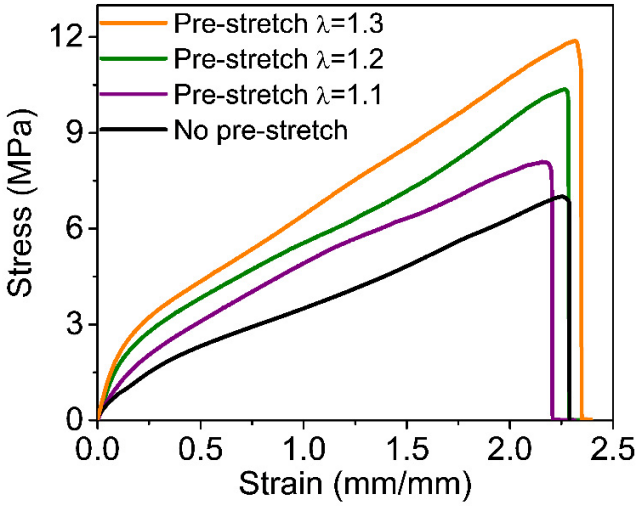

Figure S30. Stress-strain curves of experimental polymer samples (with free NCO groups and embedded chloroplasts) with various pre-stretches after the photosynthesis process (4-h light and 4-h darkness).

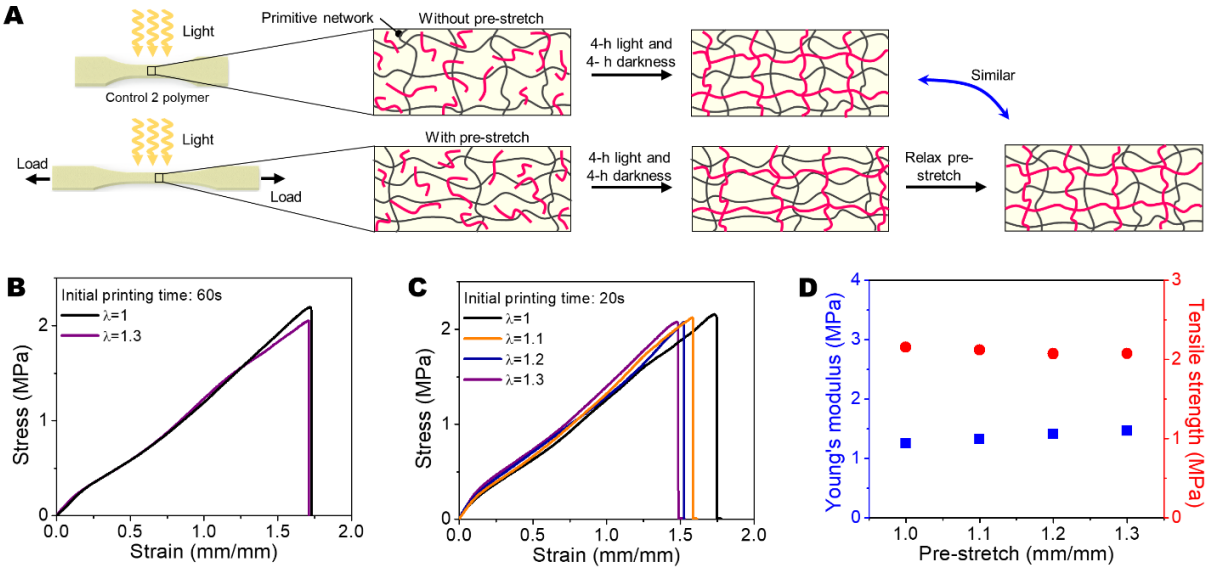

Figure S31. Effect of pre-stretch on the mechanical property of post-cured control 2 polymer (with free NCO groups but without chloroplasts). (A) Schematics to illustrate the post-curing of control 2 samples without and with a pre-stretch. The post-curing condition is the same as the photosynthesis condition: 4-h light illumination and 4-h darkness. (B) Stress-strain curves of post-cured control 2 samples (printed with 60 s, close to fully cured) without a pre-stretch and with a pre-stretch of 1.3. (C) Stress-strain curves of post-cured control 2 samples (printed with 20 s, partially-cured) without a pre-stretch ($\lambda = 1$) and with various pre-stretches ($\lambda = 1.1 - 1.3$). (D) The Young's moduli and tensile strengths of the post-cured control 2 samples (printed with 20 s, partially-cured) in functions of the pre-stretch λ.

Experimental procedure: The samples were prepared by 3D printing process using control 2 polymer ink (with free NCO groups but without chloroplasts) under different light exposure time (20 s or 60 s). When the light exposure time was 60 s, the sample was fully crosslinked; when the light exposure time was 20 s, the sample was partially-cured. The fabricated samples were then uniaxially pre-stretched with various stretches ($\lambda = 1 - 1.3$) and undergone 4-h light illumination and 4-h darkness. The pre-stretched section of the samples was then cut into dumbbell-like shape, and uniaxially stretched until rupture with a strain rate of 0.05 s^{-1}.

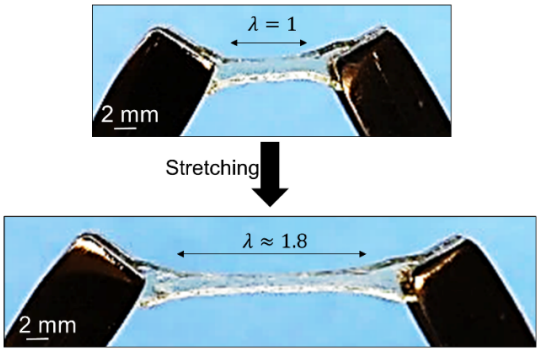

Figure S32. Stretching of a healed sample after 4-h light illumination and 4-h darkness.

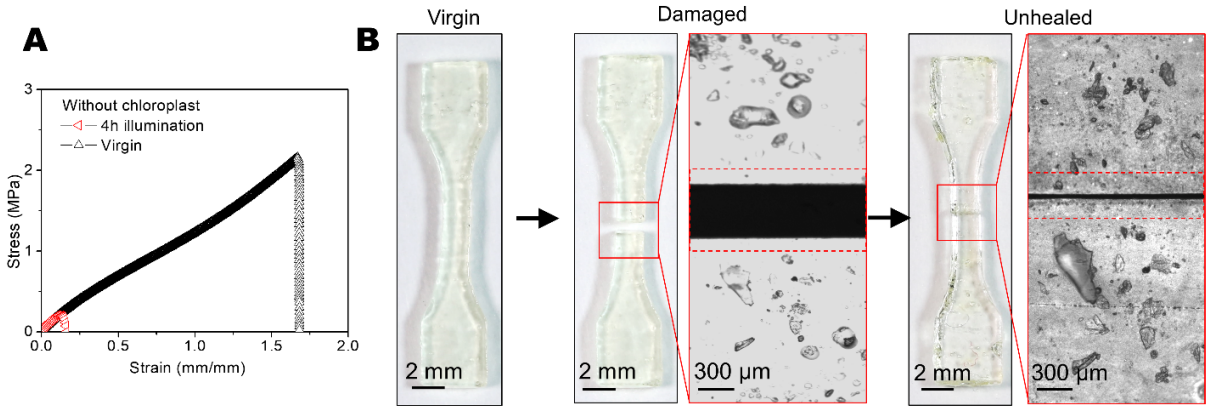

Figure S33. **Self-healing of the control sample**. (A) Uniaxial tensile stress-strain curves of control samples with free NCO groups but without embedded chloroplasts at the virgin state and after the healing process (4-h illumination and 4-h darkness). (B) control samples and interfacial microscope images at the virgin, damaged, and healed states.

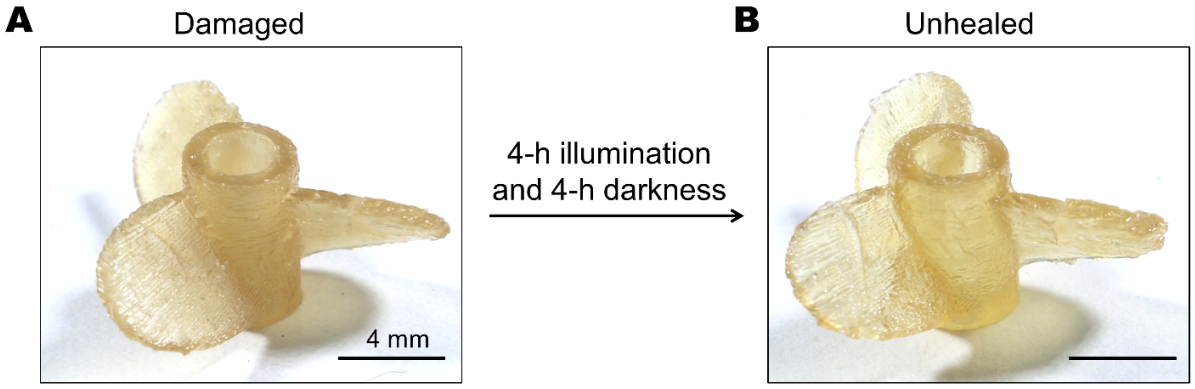

Figure S34. Healing process of 3D-printed propeller made by control 2 polymer with free NCO group but without embedded chloroplasts. (A) Image of sample damaged with sharp blade (B) Image of the unhealed sample after 4-h light illumination and 4-h darkness. The scale bars represent 4 mm.

Table S1.

Experimental data for measuring the mass percentage of water within the extracted chloroplast.

Sample #	The initial mass of extracted chloroplast (g)	Mass after 8-h evaporation in a dark environment (g)	Mass of water (g)	Mass percentage of water (%)
1	0.3092	0.0592	0.25	80.9
2	0.3019	0.0529	0.249	82.5
3	0.3097	0.0567	0.253	81.7
4	0.3042	0.0452	0.259	85.1
5	0.3	0.041	0.259	86.3
6	0.3075	0.0405	0.267	86.8
			Mean	83.9
			Standard deviation	2.5

Table S2.
Parameters used for the theoretical calculations.

Parameter	Physical meaning	Figs. S22AB	Figs. S22CD
N_0	Initial chain length	400	400
n_0	Initial chain number density (m^{-3})	4.5×10^{19}	4.5×10^{19}
T	Temperature (K)	300	300
n_a/n_0	Normalized additional crosslink density	0 for 0% 0.6 for 1% 1.1 for 3% 2.1 for 5%	0 for 0 h 0.5 for 0.25 h 1 for 0.5 h 1.8 for 1 h 2.3 for 2h

Movie S1.

A movie to illustrate the photosynthesis-assisted healing of a dumbbell-shaped sample. The sample was 3D-printed with a polymer ink with free NCO groups and 5 wt% embedded chloroplasts. Then, the sample was cut into two parts with a blade, followed by being brought into contact under 4-h light illumination and 4-h darkness. Then the healed sample was stretched by two twisters.

Movie S2.

A movie to illustrate the comparison of 3D-printed experimental and control propellers in healing fractures in their structures. In the first part, a 3D-print propeller with the experimental polymer ink with free NCO groups and 5 wt% embedded chloroplasts was damaged by making cracks in its sectors. The sector cracks were healed by a photosynthesis process with 4-h illumination and 4-h darkness. The healed propeller that was assembled on a remotely controlled boat could facilitate the forward movement of the boat. In the second part, a 3D-print propeller with the control polymer ink with free NCO groups but without embedded chloroplasts was damaged by making cracks on its sectors. The sector cracks could not be healed by a photosynthesis process with 4-h illumination and 4-h darkness. The unhealed propeller that was assembled on a remotely controlled boat could not facilitate the forward movement of the boat.

References

1 Treloar, L. R. G. *The physics of rubber elasticity*. (Oxford University Press, USA, 1975).

2 Arruda, E. M. & Boyce, M. C. A three-dimensional constitutive model for the large stretch behavior of rubber elastic materials. (1993).

3 Rubinstein, M. & Colby, R. H. *Polymer physics*. Vol. 23 (Oxford university press New York, 2003).

4 Yu, K., Xin, A., Feng, Z., Lee, K. H. & Wang, Q. Mechanics of self-healing thermoplastic elastomers. *Journal of the Mechanics and Physics of Solids* **137**, 103831 (2020).

5 Xin, A., Zhang, R., Yu, K. & Wang, Q. Mechanics of electrophoresis-induced reversible hydrogel adhesion. *Journal of the Mechanics and Physics of Solids* **125**, 1-21 (2019).

6 Yu, K., Xin, A. & Wang, Q. Mechanics of light-activated self-healing polymer networks. *Journal of the Mechanics and Physics of Solids* **124**, 643-662 (2019).

7 Yu, K., Xin, A. & Wang, Q. Mechanics of self-healing polymer networks crosslinked by dynamic bonds. *Journal of the Mechanics and Physics of Solids* **121**, 409-431 (2018).

8 Wang, Q., Gao, Z. & Yu, K. Interfacial self-healing of nanocomposite hydrogels: Theory and experiment. *Journal of the Mechanics and Physics of Solids* **109**, 288-306 (2017).

9 Wang, Q. & Gao, Z. A constitutive model of nanocomposite hydrogels with nanoparticle crosslinkers. *Journal of the Mechanics and Physics of Solids* **94**, 127-147 (2016).

10 Wang, Q., Gossweiler, G. R., Craig, S. L. & Zhao, X. Mechanics of mechanochemically responsive elastomers. *Journal of the Mechanics and Physics of Solids* **82**, 320-344 (2015).

11 Joly, D. & Carpentier, R. in *Photosynthesis Research Protocols* Vol. 684 (ed Robert Carpentier) 321-325 (Humana Press, 2011).

12 Von Caemmerer, S. *Biochemical models of leaf photosynthesis*. (Csiro publishing, 2000).

13 Lawlor, D. W. *Photosynthesis: molecular, physiological and environmental processes*. (Longman scientific & technical, 1993).

14 Gregory, R. P. F. *Biochemistry of photosynthesis*. Vol. 5 (Wiley London, 1977).

15 Matsunaga, K., Sato, K., Tajima, M. & Yoshida, Y. Gas permeability of thermoplastic polyurethane elastomers. *Polymer journal* **37**, 413-417 (2005).

16 Xiao, H., Ping, Z. H., Xie, J. W. & Yu, T. Y. Permeation of CO2 through polyurethane. *Journal of Applied Polymer Science* **40**, 1131-1139 (1990).

17 https://www.co2.earth/daily-co2.

18 Korolevich, M. V., Zhbankov, R. G. & Sivchik, V. V. Calculation of absorption-band frequencies and intensities in the ir-spectrum of alpha-d-glucose in a cluster. *Journal of Molecular Structure* **220**, 301-313 (1990).